Cellular Distribution of the Fragile X Mental Retardation Protein in the Mouse Brain

Diego A.R. Zorio,[1] Christine M. Jackson,[1] Yong Liu,[1] Edwin W. Rubel,[2] and Yuan Wang[1,3]*

[1]Department of Biomedical Sciences, College of Medicine, Florida State University, Tallahassee, Florida, USA
[2]Virginia Merrill Bloedel Hearing Research Center, Department of Otolaryngology-Head and Neck Surgery, University of Washington School of Medicine, Seattle, Washington, USA
[3]Program in Neuroscience, Florida State University, Tallahassee, Florida, USA

ABSTRACT

The fragile X mental retardation protein (FMRP) plays an important role in normal brain development. Absence of FMRP results in abnormal neuronal morphologies in a selected manner throughout the brain, leading to intellectual deficits and sensory dysfunction in the fragile X syndrome (FXS). Despite FMRP importance for proper brain function, its overall expression pattern in the mammalian brain at the resolution of individual neuronal cell groups is not known. In this study we used FMR1 knockout and isogenic wildtype mice to systematically map the distribution of FMRP expression in the entire mouse brain. Using immunocytochemistry and cellular quantification analyses, we identified a large number of prominent cell groups expressing high levels of FMRP at the subcortical levels, in particular sensory and motor neurons in the brainstem and thalamus. In contrast, many cell groups in the midbrain and hypothalamus exhibit low FMRP levels. More important, we describe differential patterns of FMRP distribution in both cortical and subcortical brain regions. Almost all major brain areas contain high and low levels of FMRP cell groups adjacent to each other or between layers of the same cortical areas. These differential patterns indicate that FMRP expression appears to be specific to individual neuronal cell groups instead of being associated with all neurons in distinct brain regions, as previously considered. Taken together, these findings support the notion of FMRP differential neuronal regulation and strongly implicate the contribution of fundamental sensory and motor processing at subcortical levels to FXS pathology. J. Comp. Neurol. 525:818–849, 2017.

INDEXING TERMS: fragile X syndrome; whole brain analyses; cortical laminar heterogeneity; subcortical sensory systems; sensory information processing; RRID:AB_10805421; RRID:AB_1157880; RRID:AB_476743

Loss of the fragile X mental retardation protein (FMRP) leads to fragile X syndrome (FXS) in children, the leading known genetic cause of autism spectrum disorders (Verkerk et al., 1991; Penagarikano et al., 2007; Bagni et al., 2012; Santoro et al., 2012). FMRP is encoded by the X-linked gene FMR1. Transcriptional silencing of FMR1 leads to loss of FMRP protein and abnormal neuronal structure and function (Rudelli et al., 1985; Hinton et al., 1991; Braun and Segal, 2000; Irwin et al., 2001, 2002; Galvez et al., 2003, 2005; McKinney et al., 2005; Levenga et al., 2011; Till et al., 2012). Phenotypically, patients exhibit intellectual disability including learning and memory deficits, communication and social difficulties, as well as sensory and motor dysfunction. Consistent with these observations, FMRP is highly expressed in healthy brains, particularly in neuronal structures (Devys et al., 1993; Hinds et al., 1993; Gholizadeh et al., 2015).

To explore FMRP mechanisms in normal brain development and function, as well as the contribution of FMRP loss to FXS phenotypes, it is important to understand the expression patterns of FMRP in the brain. Earlier studies reported intensive FMRP expression in the hippocampus, cerebellum, nucleus basalis, cerebral cortex, and olfactory bulb, while reporting minimal or

Grant sponsor: National Institute on Deafness and Other Communication Disorders; Grant number: DC-013074.

*CORRESPONDENCE TO: Yuan Wang, Department of Biomedical Sciences, Florida State University, 1115 West Call St., Tallahassee, FL 32306. E-mail: yuan.wang@med.fsu.edu

Received April 21, 2016; Revised August 10, 2016;
Accepted August 11, 2016.
DOI 10.1002/cne.24100
Published online September 16, 2016 in Wiley Online Library (wileyonlinelibrary.com)

generally low levels of FMRP in other brain areas such as corpus callosum, brainstem, and thalamus (Hinds et al., 1993; Devys et al., 1993; Abitbol et al., 1993; Bakker et al., 2000; Zangenehpour et al., 2009). More recent studies, however, demonstrated that FMRP is distributed throughout the brain and is expressed in most, if not all, neurons (Feng et al., 1997; Christie et al., 2009). In certain cases, the expression level of FMRP appears highly heterogeneous. Hinds et al. (1993) reported a "dense yet patchy" labeling pattern of FMR1 hybridization in the mouse cortex. In the visual thalamus, a high FMRP expression level is detected in the magnocellular, but not parvocellular, neurons of the primate lateral geniculate nucleus (Kogan et al.,

ABBREVIATIONS

ACA	Anterior cingulate area
ACB	Nucleus accumbens
aco	Anterior commissure, olfactory limb
AOB	Accessory olfactory bulb
AON	Anterior olfactory nucleus
BAC	Bed nucleus of the anterior commissure
BLA	Basolateral amygdalar nucleus
BMA	Basomedial amygdalar nucleus
BMAa	Basomedial amygdalar nucleus, anterior part
BMAp	Basomedial amygdalar nucleus, posterior part
CA1	Field CA1
CA3	Field CA3
ccg	Genu of corpus callosum
CEA	Central amygdalar nucleus
CLA	Claustrum
COA	Cortical amygdalar area
CP	Caudoputamen
cst	Corticospinal tract
CU	Cuneate nucleus
DCO	Dorsal cochlear nucleus
DG	Dentate gyrus
DMH	Dorsomedial nucleus of the hypothalamus
DMX	Dorsal motor nucleus of the vagus nerve
DN	Dentate nucleus
ECU	External cuneate nucleus
EP	Endopiriform nucleus
fa	Corpus callosum, anterior forceps
FN	Fastigial nucleus
fr	Fasciculus retroflexus
GP	Globus pallidus
GR	Gracile nucleus
GRN	Gigantocellular reticular nucleus
gVIIn	Genu of the facial nerve
IA	Intercalated amygdalar nucleus
IC	Inferior colliculus
ICc	Inferior colliculus, central nucleus
ICe	Inferior colliculus, external nucleus
IGL	Intergeniculate leaflet of the lateral geniculate complex
IO	Inferior olivary complex
IP	Interposed nucleus
IRN	Intermediate reticular nucleus
isl	Islands of Calleja
LA	Lateral amygdalar nucleus
LAV	Lateral vestibular nucleus
LGd	Dorsal part of the lateral geniculate complex
LGv	Ventral part of the lateral geniculate complex
LH	Lateral habenula
LM	Lateral mammillary nucleus
LP	Lateral posterior nucleus of the thalamus
LRNm	Lateral reticular nucleus, magnocellular part
LSc	Lateral septal nucleus, caudal (caudodorsal) part
LSO	Lateral superior olive
LSr	Lateral septal nucleus, rostral (rostroventral) part
LSv	Lateral septal nucleus, ventral part
MARN	Magnocellular reticular nucleus
MEA	Medial amygdalar nucleus
MEApv	Medial amygdalar nucleus, posteroventral part
MEV	Midbrain trigeminal nucleus
MG	Medial geniculate complex
MH	Medial habenula
MM	Medial mammillary nucleus
MMl	Medial mammillary nucleus, lateral part
MMm	Medial mammillary nucleus, medial part
MOB	Main olfactory bulb
MOBgl	Main olfactory bulb, glomerular layer
MOBgr	Main olfactory bulb, granule layer
MOBmi	Main olfactory bulb, mitral layer
MOBopl	Main olfactory bulb, outer plexiform layer
moV	Motor root of the trigeminal nerve
MSO	Medial superior olive
MV	Medial vestibular nucleus
NDB	Diagonal band nucleus
NLL	Nucleus of the lateral lemniscus
NLLd	Nucleus of the lateral lemniscus, dorsal part
NLLh	Nucleus of the lateral lemniscus, horizontal part
NLLv	Nucleus of the lateral lemniscus, ventral part
NLOT	Nucleus of the lateral olfactory tract
NTB	Nucleus of the trapezoid body
NTS	Nucleus of the solitary tract
och	Optic chiasm
OT	Olfactory tubercle
PA	Posterior amygdalar nucleus
PAG	Periaqueductal gray
PAR	Parasubiculum
PALv	Pallidum, ventral region
PBG	Parabigeminal nucleus
PF	Parafascicular nucleus
PG	Pontine gray
PIR	Piriform area
PMv	Ventral premammillary nucleus
PO	Posterior complex of the thalamus
POST	Postsubiculum
PRE	Presubiculum
PRN	Pontine reticular nucleus
PRP	Nucleus prepositus
PSTN	Parasubthalamic nucleus
PSV	Principal sensory nucleus of the trigeminal
py	Pyramid
RN	Red nucleus
RO	Nucleus raphe obscurus
RPA	Nucleus raphe pallidus
RSPd	Retrosplenial area, dorsal part
SC	Superior colliculus
SCig	Superior colliculus, motor related, intermediate gray layer
SCiw	Superior colliculus, motor related, intermediate white layer
SCm	Superior colliculus, motor related
SCop	Superior colliculus, optic layer
SCs	Superior colliculus, sensory related
SCsg	Superior colliculus, superficial gray layer
SCzo	Superior colliculus, zonal layer
SEZ/RC	subependymal zone
SF	Septofrimbrial nucleus
sm	Stria medullaris
SNc	Substantia nigra, compact part
SNr	Substantia nigra, reticular part
SOC	Superior olivary complex
SPIV	Spinal vestibular nucleus
SPO	Superior paraolivary nucleus
SPV	Spinal nucleus of the trigeminal
SS	Primary somatosensory area
STN	Subthalamic nucleus
SUM	Supramammillary nucleus
SUV	Superior vestibular nucleus
TMv	Tuberomammilliary nucleus, ventral part
TRN	Tegmental reticular nucleus
TU	Tuberal nucleus
V	Motor nucleus of the trigeminal
VCO	Ventral cochlear nucleus
VENT	Ventral group of the dorsal thalamus
VI	Abducens nucleus
VII	Facial motor nucleus
VIIn	Facial nerve
VIS	Primary visual area
VL	Lateral ventricle
VNC	Vestibular nuclei
VP	Ventral posterior complex of the thalamus
VPM	Ventral posteromedial nucleus of the thalamus
VTA	Ventral tegmental area
XII	Hypoglossal nucleus

2004a). Importantly, this difference is consistent with selective visual deficits of the magnocellular pathway in FXS individuals (Kogan et al., 2004a,b). In the brainstem, our recent studies have identified high levels of FMRP in auditory neurons as compared to other neuronal cell types in adjacent areas (Beebe et al., 2014; Wang et al., 2014), which is consistent with other reports in FMR1 knockout mice showing reduced cell size, altered synaptic connectivity, and reduced dynamics in ion channel regulation of auditory brainstem neurons (Strumbos et al., 2010; Rotschafer et al., 2015). In addition, reduced FMR1 expression leads to structural abnormalities of dendritic spines in the hippocampus CA1, but not CA3 (Levenga et al., 2011). These studies emphasize the importance of identifying FMRP-rich neuronal cell types in normal brains, as they could potentially be the prominent targets of FMRP loss and thus reasonable candidates for exploring FXS pathology.

Although systematic maps of a specialized presynaptic format of FMRP has been previously reported (Christie et al., 2009; Akins et al., 2012), the overall FMRP distribution in the entire mammalian brain at the resolution of individual neuronal cell groups is not known. Using immunocytochemistry, the current study provides a detailed analysis of FMRP distribution in the whole brain of FVB mice, as the FMR1 knockout strain on this genetic background is commonly used for studying FMRP loss-induced neuronal deficits and for testing drug candidates for rescuing FXS phenotypes (for example, Bakker et al., 1994; Fisch et al., 1999; Chen and Toth, 2001; Irwin et al., 2002; Strumbos et al., 2010; La Fata et al., 2014). When compared to their isogenic wildtype mice, FMR1 knockout mice on FVB background exhibit volume changes in more brain regions than FMR1 knockout mice on C57BL/6 background (Lai et al., 2016) and they show more dramatic behavioral alterations (Pietropaolo et al., 2011).

The data presented in this study identify a number of distinct neuronal cell types that are particularly rich in FMRP at the subcortical levels, as well as differential patterns of FMRP distribution in both the cortical and subcortical brain regions.

MATERIALS AND METHODS

Animals

FMR1 knockout (Hemi FVB.129P2-Pde6b+; #004624) mice and their wildtype littermates (FVB.129P2-Pde6b+; #004828) were purchased from the Jackson Laboratory (Bar Harbor, ME). Six wildtype and four knockout animals of 5–6 weeks old were used in this study. All procedures were approved by the Florida State University Institutional Animal Care and Use Committee and conformed to National Institutes of Health (NIH) guidelines.

Immunocytochemistry

The animals were anesthetized with a mixture of 100 mg/kg ketamine and 15 mg/kg xylazine and transcardially perfused with 0.9% saline followed by 4% paraformaldehyde in 0.1 M phosphate buffer (PB). The brains were removed from the skull and postfixed overnight in the same fixative. The brains were then transferred to 30% sucrose in PB until they sank, frozen on the stage of a sliding microtome, and then sectioned either coronally (three wildtype and two knockout) or parasagittally (three wildtype and two knockout) at 30 μm. Sections were collected in 0.01 M phosphate-buffered saline (PBS) into four alternate sets of serial sections and stained for Nissl substance or immunocytochemistry.

For FMRP immunostaining, the sections were mounted on gelatin-coated slides and dried at 37°C overnight. Sections were then washed in PBS for 15 minutes, pretreated with 0.1% sodium borohydride in PBS for 10 minutes, washed in PBS for 15 minutes, incubated in heated 10 mM citrate buffer (pH 6.0) for 20 minutes in a water steamer, washed in PBS for 10 minutes, followed by 50 mM ammonium chloride in PBS for 15 minutes, then finally washed in PBS for 10 minutes. Sections were then incubated with primary antibody solutions diluted 1:500 in PBS with 0.3% Triton X-100 overnight at 4°C, followed by biotinylated goat anti-IgG antibodies (1:200; Vector Laboratories, Burlingame, CA) for 1 hour at room temperature. Sections were incubated in avidin-biotin-peroxidase complex solution (ABC Elite kit; Vector Laboratories) diluted 1:100 in PBS with 0.3% Triton X-100 for 1 hour at room temperature. For visualization, sections were incubated for 3–7 minutes in 0.015% 3-3′-diaminobenzidine (Sigma, St. Louis, MO), either with 0.01% hydrogen peroxide in PB or with 0.03% hydrogen peroxide, 125 mM sodium acetate, 10 mM imidazole, and 100 mM nickel ammonium sulfate. Sections were then dehydrated, cleared, and coverslipped with DPX mounting medium (EMS, Hatfield, PA).

Antibody characterization

A number of monoclonal and polyclonal antibodies have been produced to detect FMRP. All of these antibodies detect FMRP bands on Western blot. However, many of them are not specific, as evidenced by extra bands on Western blot in addition to FMRP. While these antibodies provide a useful tool for Western blot and immunoprecipitation studies which separate FMRP from other proteins of different molecular weights or

TABLE 1.
Primary Antibodies Used for Immunocytochemistry (ICC) and Western Blots (WB)

	Antigen	Host, monoclonal or polyclonal, dilution	Manufacturer, catalog number
7G1	amino acid 354-368 (KHLDTKENTHFSQPN) of mouse FMRP-6X-his fusion protein	mouse, monoclonal, 1:500 (ICC); 1:500 (WB)	Developmental Studies Hybridoma Bank (DSHB) at the University of Iowa (Iowa City, IA)
2F5	amino acid 1-204 (N-terminus) of human FMRP-6X-His-tagged fusion protein	mouse, monoclonal, 1:500 (ICC); 1:775 (WB)	DSHB (Iowa City, IA)
β-actin	slightly modified β-cytoplasmic actin N-terminal peptide, G, conjugated to KLH	mouse, monoclonal, 1:5000 (WB)	Sigma, A5316

structure, they are less useful for studying cellular and subcellular protein localization in intact tissue samples using immunocytochemistry. Out of 13 commercially available anti-FMRP antibodies tested in our lab, we chose two antibodies, 7G1 and 2F5, to use for immunocytochemistry, as they show the most specific detection of the mouse FMRP in both Western blot and immunocytochemistry.

Monoclonal anti-FMRP antibody 7G1 was first generated by Brown et al. (2001) by immunizing FMR1 knockout mice with hexahistidine-tagged FMRP. The FMRP-epitope recognized by 7G1 is amino acid 354–368 of the mouse FMRP, in a region with no homology to the fragile X-related paralogs. The specificity of the antibody was characterized by Western blot in Brown et al. (2001) and further tested by both Western blot and immunocytochemistry in the current study (see Results).

Monoclonal anti-FMRP antibody 2F5 was produced by Gabel et al. (2004) by immunizing FMR1 knockout mice with an N-terminal fragment of human FMRP (residues 1–204). Immunocytochemical and Western blot analyses of wildtype and FMR1 knockout mice demonstrate that 2F5 is specific for FMRP, as first characterized in Gabel et al. (2004) and confirmed in the current study (see Results). The 2F5 antibody used in the current study was initially provided generously by Dr. Jennifer Darnel at the Rockefeller University and then purchased from the Developmental Studies Hybridoma Bank (DSHB, Iowa City, IA).

It is worthy to note that neither 7G1 nor 2F5 reveals substantial dendritic staining by light microscopy, except of the most proximal part of dendrites in some, but not all, neurons. Our previous study with a polyclonal antibody ab17722 (Abcam; San Francisco, CA) reveals prominent FMRP clusters throughout dendritic branches in the brainstem (Wang et al., 2014). Unfortunately, subsequent batches of the antibody lost specificity when compared to the first batch that we used, exhibiting non-FMRP staining throughout the FMR1 knockout mouse brain. Due to limited visualization of dendritic staining, the current study focuses on the description of somatic FMRP staining.

Mouse monoclonal anti-β-actin was used as a loading control in Western blot analysis. This antibody recognizes an epitope located on the N-terminal end of the β-isoform of actin. It specifically labels β-actin in a wide variety of tissues and species, as tested by Western blot (manufacturer's data sheet) and on mouse brains in the current study.

The optimal antibody concentration was obtained by running a series of concentration tests to avoid floor or ceiling truncation, including a negative control by omitting primary antibody. Immunogen, host species, clone type, manufacturer's information, as well as dilution used for each antibody in each species, are listed in Table 1.

Western blot

Protein samples were harvested from flash-frozen brain tissue from wildtype and FMR1 knockout mice. Samples were homogenized in EDTA buffer (62.5 mM Tris-HCl pH 6.8, 2% sodium dodecyl sulfate [SDS], 10% glycerol, 5% β-ME, 10 mM EDTA) using the Ultra-Turrax T10 homogenizer (IKA Works, Wilmington, NC). For each sample, 50 μg of protein in SDS buffer (2% SDS, 50 mM Tris pH 7.6, 5% glycerol and 0.025% bromophenol blue) was incubated at 70°C for 10 minutes, resolved in NuPAGE 4–12% Bis-Tris Gels (Life Technologies, Carlsbad, CA), and then transferred onto PDVF membranes (GE Healthcare, Chicago, IL). After blocking in 5% milk in PBS with 0.05% Tween (PBS-T) for 30 minutes at room temperature, membranes were probed against a primary anti-FMRP antibody or β-actin for loading control overnight at 4°C in 1% milk in PBS-T. Specific secondary horseradish peroxidase (HRP)-conjugated antibodies were used at 1:2,500 dilution (Santa Cruz, Biotechnology, Dallas, TX) and blots were developed with SuperSignal West Pico Chemiluminescent Substrate (Thermo Scientific, Waltham, MA) and exposed to X-ray film.

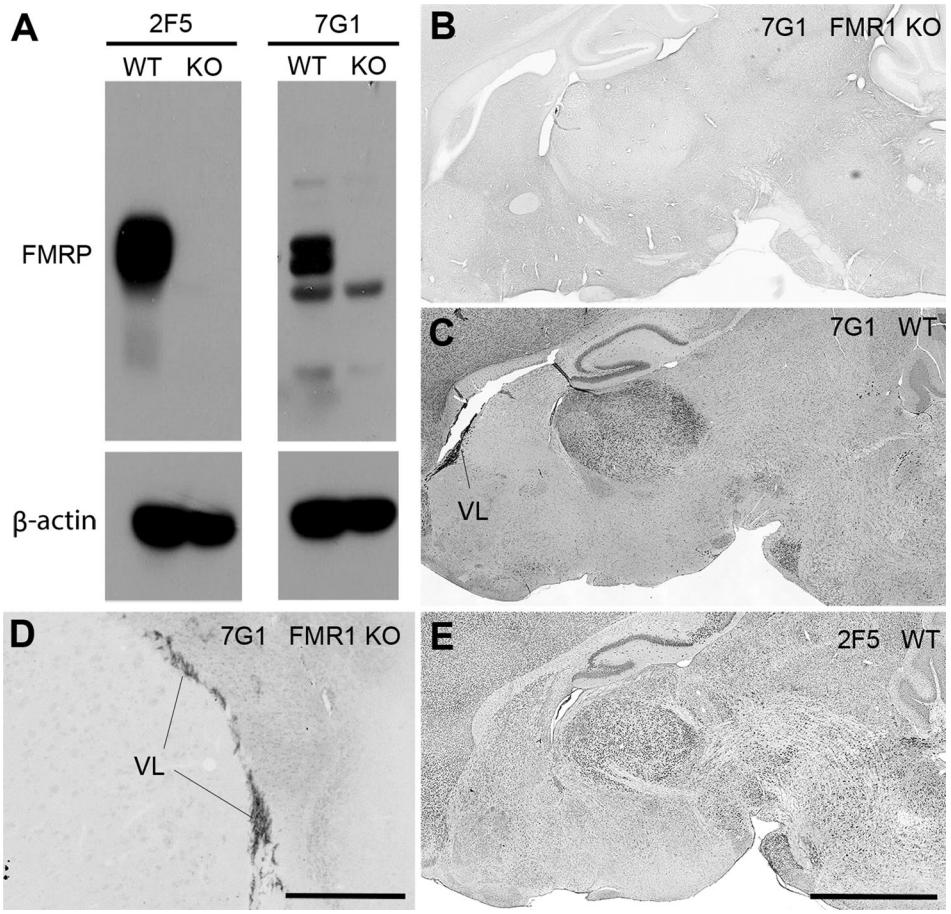

Figure 1. Antibody characterization for FMRP in the mouse brain. **A**: Western blot of 2F5 and 7G1 on brain samples from wildtype (WT) and FMR1 knockout (KO) mice. Fifty μg of protein was loaded to each lane with β-actin as the loading control. **B–D**: 7G1 immunostaining in the WT (C) and FMR1 KO (B,D) mouse brain. Note the nonspecific staining in the lateral ventricle (VL; D). **E**: 2F5 immunostaining in the WT mouse brain. Scale bars = 2 mm in E (applies to B,C,E); 500 μm in D.

Data analysis

From each brain, every fourth section was stained for 7G1 immunoreactivity, 2F5 immunoreactivity, and Nissl. For each set of staining, there were a total of 105–115 coronal sections from the spinal cord to the olfactory bulb or 50–60 parasagittal sections from the lateral surface to the midline. To avoid staining variations across slides and sections, sections within the same series were treated the same way and simultaneously whenever possible. For each section, image tiles were captured at 16 bits with a 20× lens and an Axiocam 503 color camera mounted on a Zeiss Imager M2 microscope. While imaging, an autofocus function in the Zeiss Zen software was applied to ensure all image tiles were in focus. The image tiles were then montaged using the titling function of the Zeiss Zen software. This imaging protocol generated a single image of the entire section at a high resolution. All sections were captured and subsequently processed using the same parameters, so that the optical density of the background was within 1% deviation across images. Here the background is referred to a region on the slide without brain tissue present. Image brightness and contrast adjustments were performed using Adobe PhotoShop (Adobe Systems, Mountain View, CA). All drawings were produced in Adobe Illustrator (Adobe Systems).

All subsequent quantitative analyses were based on measurements from 7G1 immunostaining. To reveal FMRP-rich cells throughout the mouse brain, we performed a pixel-based threshold analysis. The tiled image of an entire section was converted to 8 bit in black and white and used to generate a threshold image at the pixel brightness point of 114 using Fiji software (v. 1.50e; National Institutes of Health, Bethesda, MD). This threshold was chosen to reveal high intensities of FMRP staining and was applied to all sections analyzed.

To compare FMRP expression levels between cell groups, we performed an intensity analysis on FMRP immunostaining at the individual cell level in 85 selected neuronal cell groups. For each cell group, all 7G1-labeled coronal sections containing a significant portion of this cell group were identified. The most middle sections through each cell group were used to determine the cells to be measured based on the following criteria: 1) its location can be unambiguously identified within the border of the cell group; 2) this cell has an identifiable cell boundary and a well-defined nucleus; and 3) the cross-sectional cell body area of this cell is

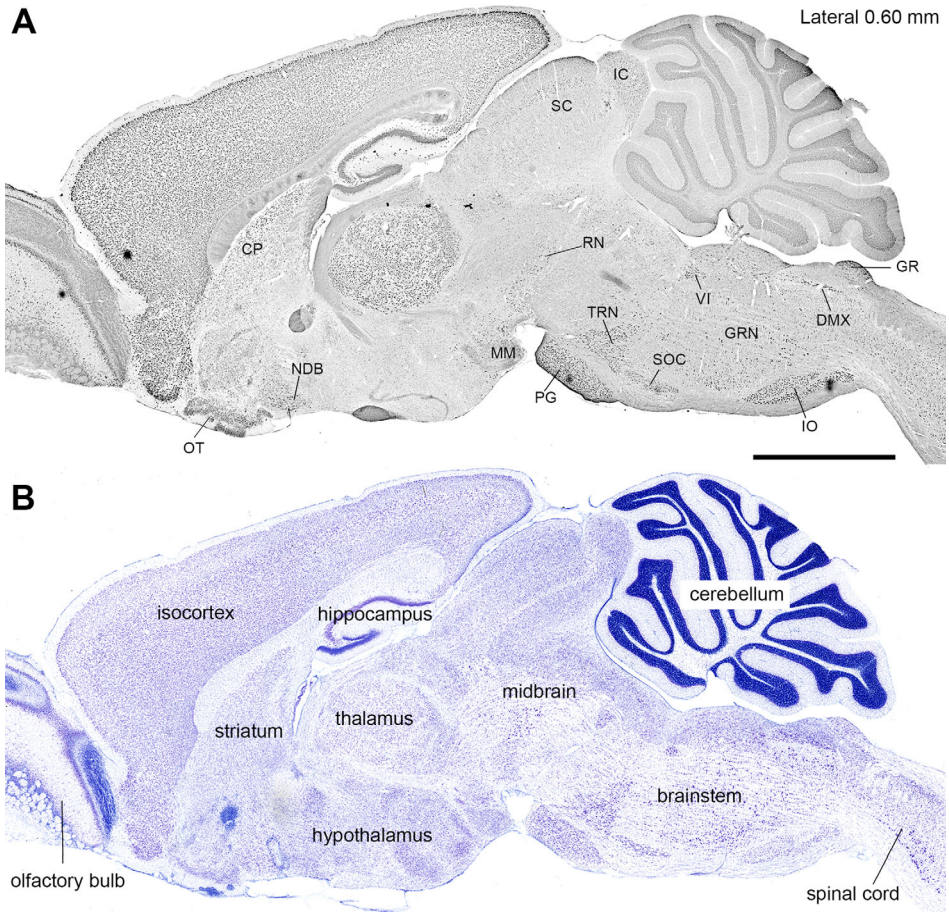

Figure 2. FMRP (7G1) immunostaining in the sagittal plane at the medial level of the wildtype mouse brain. This level is comparable to Lateral 0.60 mm according to the Mouse Brain Atlas (Paxinos and Franklin, 2013). The 7G1 immunostaining (**A**) and the Nissl stain (**B**) were taken from two sections at the comparable level. Note differential FMRP levels across brain regions, high in the olfactory bulb, cerebral cortex, hippocampus, thalamus, and cerebellum, and generally low in the hypothalamus and midbrain. The brainstem contains many distinct cell groups that are rich in FMRP. Scale bar = 2 mm. [Color figure can be viewed at wileyonlinelibrary.com]

more than 40 μm^2. To analyze a minimum of 30 cells from each cell group, a single section was used for large cell groups, while multiple sections were used for smaller cell groups. Once a section was included in the analysis for a particular cell group, all cells matching the above criteria were measured.

For each selected cell, the mean optical intensity of FMRP immunostaining within the cell body was measured in the Fiji software (v. 1.50e; NIH). After background subtraction, the optical intensity of each measured cell was normalized to the average optical intensity of all measured cells in the ventral premammillary nucleus (PMv), the cell group with the smallest average optical intensity among all measured cell groups. The background was measured in a region where there was no tissue present. Statistical analyses between cell groups were performed in the Prism software (v. 6; GraphPad Software, La Jolla, CA) using either an unpaired Student's *t*-test or one-way analysis of variance (ANOVA) followed by Tukey's multiple comparisons test. Only cell groups presented and measured from the same sections were compared statistically to minimize false positives.

To avoid individual bias in selecting cells to be measured and in outlining the border of the cell body, we selected 13 out of 85 cell groups and had them measured independently by three individual experimenters. The three sets of measurements generated demonstrate similar results in comparing FMRP staining intensity between the 13 cell groups, indicating that individual bias, if any, does not affect the main conclusion of the study. All data presented in the Results section resulted from the measurements from one experimenter.

One consideration is to what degree the cellular quantification performed here represents the entire neuronal population in the mouse brain. The goal of the current study was to provide qualitative and quantitative comparisons of FMRP expression levels across the whole brain from brainstem and midbrain to thalamus and cortex. This breadth of objectives limits the depth of the analyses. First, our description and measurements focus on the most prominent cell groups readily identifiable based on FMRP immunostaining. Therefore, neuronal cell groups that are small or without discrete borders from surrounding areas were not taken into

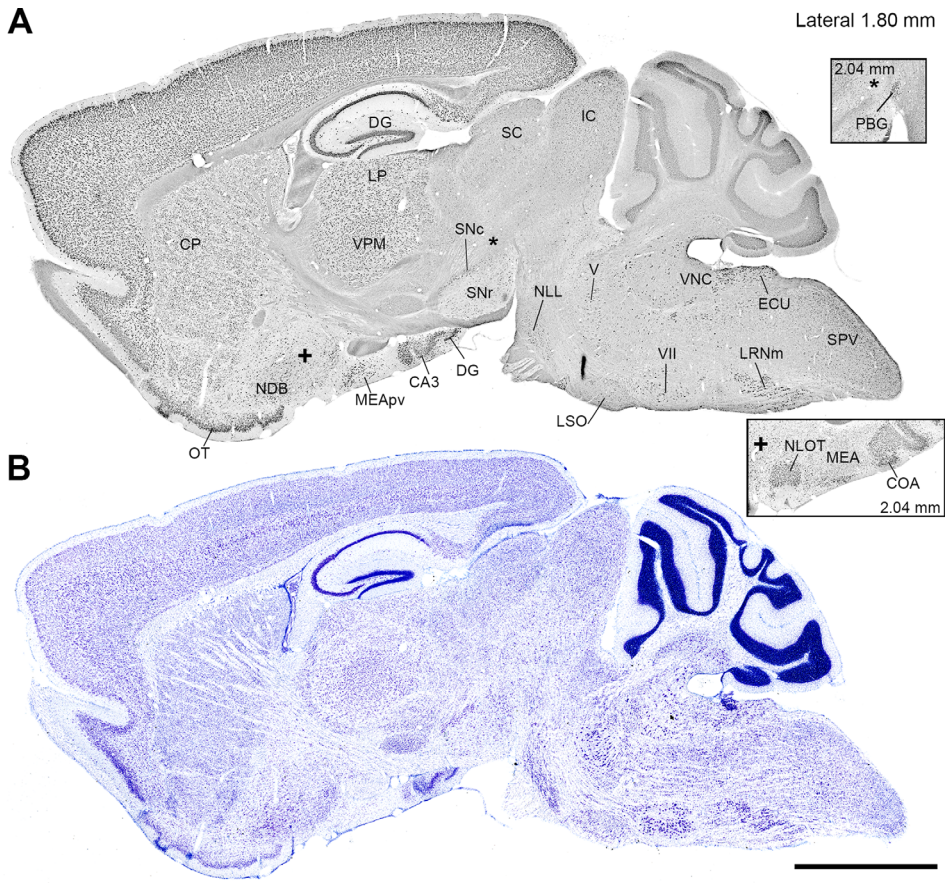

Figure 3. FMRP (7G1) immunostaining in the sagittal plane at the middle level of the wildtype mouse brain. This level is comparable to Lateral 1.80 mm according to the Mouse Brain Atlas (Paxinos and Franklin, 2013). The 7G1 immunostaining (**A**) and the Nissl stain (**B**) were taken from two sections at the comparable level. The two inserts were taken from a section at the level of Lateral 2.04 mm, corresponding to the location marked with * and +, respectively. Scale bar = 2 mm. [Color figure can be viewed at wileyonlinelibrary.com]

account. Our series of illustrations throughout the entire brain help identify some of these cell groups. For further reference, high-resolution images of FMRP (7G1) immunostaining was deposited in the Biolucida Cloud server maintained by MBF Biosciences (Williston, VT). Second, many of the cell groups selected for the analyses have heterogeneous internal organization with multiple subdivisions and/or cell types. We did not attempt to differentiate these subdivisions or cell types unless they are readily identifiable and they differ in their FMRP staining pattern. Third, our cell sampling ($n = 30$–60 neurons per cell group) is approximately from the middle of each cell group in coronal sections, rather than random sampling from the entire population of the cell group. Finally, to preferentially represent neuronal vs. glial populations, we analyzed cells with a minimal cross-sectional cell body area of 40 μm^2. This approach does not take into account neurons of smaller sizes and glial cells of larger sizes. Taken together, our analyses provide a general sampling from these cell groups, with the hope to stimulate more elaborative studies in specific brain areas in conjunction with functional studies.

RESULTS

Characterization of FMRP antibodies

Two monoclonal anti-FMRP antibodies, 7G1 and 2F5, were tested for their specificity of recognizing mouse FMRP in our preparations (Fig. 1). The antigens are located in the N-terminal and exon 11 for 2F5 and 7G1, respectively, both of which are common for the 12 mouse FMRP isoforms identified by Brackett et al. (2013). On Western blots, both antibodies detect FMRP bands on wildtype mouse brain samples (WT in Fig. 1A). These bands are absent on FMR1 knockout mouse brain samples except for a weak low-molecular band for 7G1 detection (KO in Fig. 1A). The specificity of the two antibodies was further evaluated by immunocytochemistry. Throughout the entire brain of FMR1 knockout mice, no detectable immunostaining was found for 7G1 and 2F5 antibodies (Fig. 1B) except for a strong 7G1 signal in the ependymal and subendymal layers of the lateral ventricle, sometimes called “olfactory ventricle” (Fig. 1C). Consistently, the olfactory ventricle is labeled in the wildtype mouse brain for 7G1 but not for 2F5 (Fig. 1D,E). We conclude that this 7G1 staining in the olfactory ventricle is not specific for FMRP.

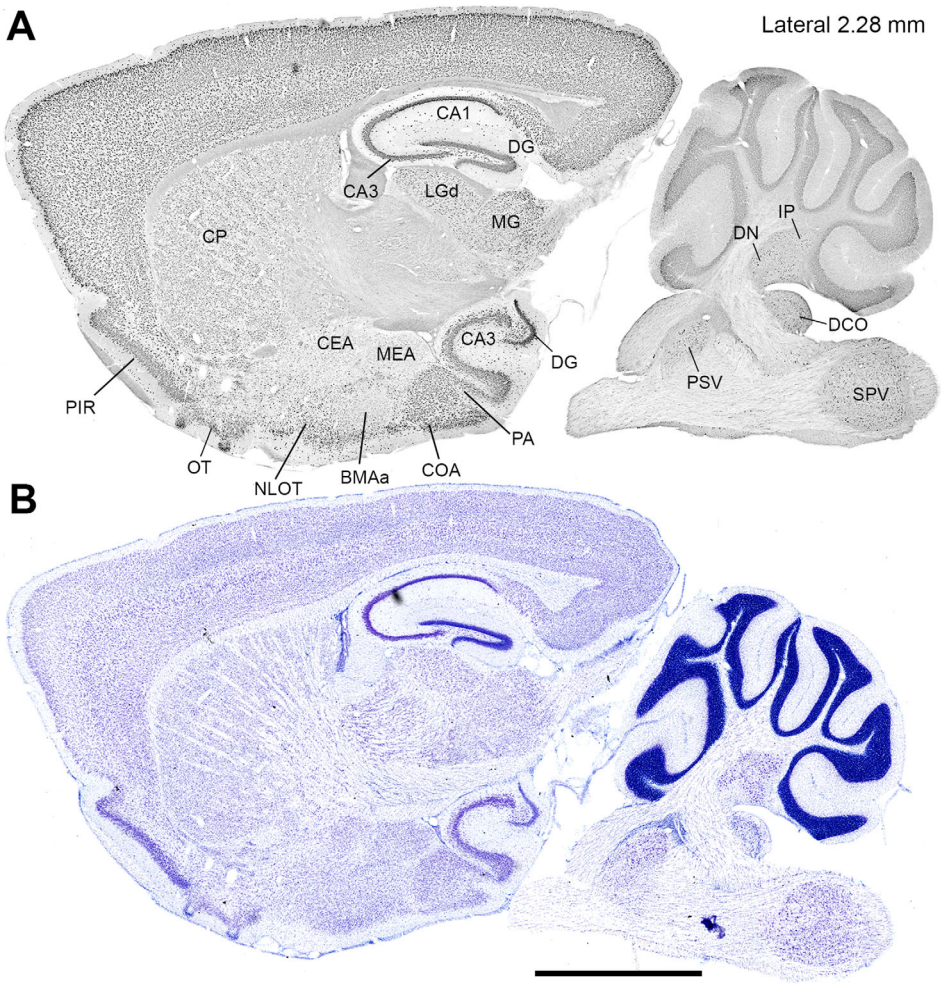

Figure 4. FMRP (7G1) immunostaining in the sagittal plane at the lateral level of the wildtype mouse brain. This level is comparable to Lateral 2.28 mm according to the Mouse Brain Atlas (Paxinos and Franklin, 2013). The 7G1 immunostaining (**A**) and the Nissl stain (**B**) were taken from two sections at the comparable level. Scale bar = 2 mm. [Color figure can be viewed at wileyonlinelibrary.com]

Except for the olfactory ventricle, the distribution pattern of the immunostaining is comparable between 7G1 and 2F5 throughout the wildtype mouse brain, consistent with the assumption that both antibodies recognize all major isoforms of the mouse FMRP. With our staining protocol, 7G1 demonstrates a larger dynamic range of immunostaining intensity than 2F5. In other words, 7G1 illustrates differential patterns of FMRP distribution across brain regions in a more dramatic manner. The subsequent description, illustrations, and quantification are thus based on 7G1 immunostaining.

General distribution pattern of FMRP immunoreactivity

Although FMRP immunoreactivity is presented throughout the entire brain, the low-magnification images nicely demonstrate that the intensity of FMRP staining varies largely across brain regions. Figures 2–4 illustrate FMRP staining on three parasagittal sections as well as Nissl stain on adjacent sections. For the purpose of description, we divide the mouse brain into seven major portions: 1) the brainstem; 2) the midbrain; 3) the cerebellum; 4) the thalamus; 5) the hypothalamus; 6) the cerebral cortex, which contains the isocortex, hippocampus, olfactory bulb, and cortical subplate; and 7) the cerebral nuclei, which contains striatum and pallidum. Consistent with a previous study (Hinds et al., 1993), the most prominent FMRP staining at low magnification is seen in the olfactory bulb, isocortex, hippocampus, thalamus, and cerebellum. In contrast, the staining level is generally low in the hypothalamus and midbrain. The entire thalamus stands out with high and relatively uniform levels of FMRP immunoreactivity, surrounded by the generally pale staining in the hypothalamus and midbrain. The brainstem, which contains a low density of neuronal cell bodies and a large number of axonal fibers as demonstrated by Nissl stain, is characterized with many distinct FMRP-rich cell groups.

Figures 5–14 illustrate FMRP staining on 12 coronal sections from caudal (the spinal cord) to rostral (the olfactory bulb). Each figure contains the original

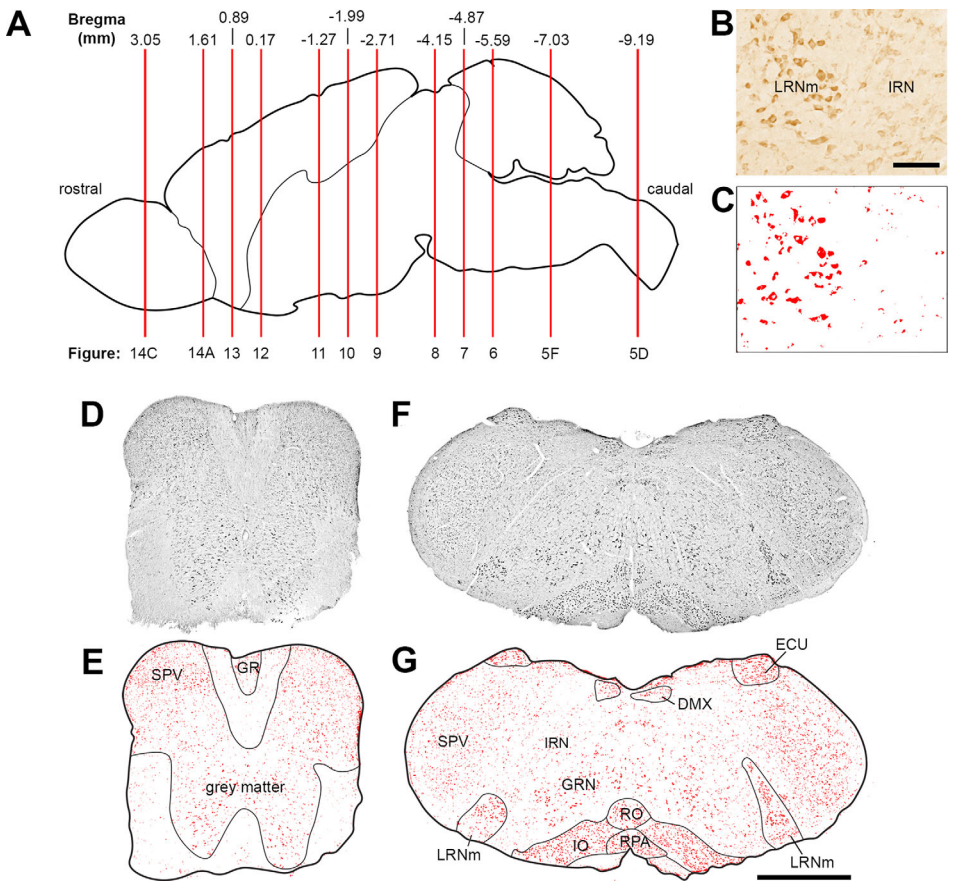

Figure 5. FMRP (7G1) immunostaining in the coronal plane through the spinal cord and caudal brainstem. **A**: Schematic drawing showing the levels of the coronal sections illustrated in Figs. 5–14 (red vertical lines). The black lines outline the mouse brain in the sagittal plane. The numerical rostral-caudal levels of each section is indicated on the top of the drawing, determined by comparing to the Mouse Brain Atlas (Paxinos and Franklin, 2013). **B,C**: An example of the original image (B) and generated threshold image (C) at a high magnification. **D,E**: The photomicrograph (D) and the threshold image (E) of 7G1 immunostaining in the spinal cord. The threshold image was generated as described in the Materials and Methods. The pixels with an optical intensity at or above the threshold are in red. The border of the brain section is outlined with black lines. **F,G**: The photomicrograph (F) and the threshold image (G) of FMRP immunostaining in the caudal brainstem at the level of the inferior olive complex (IO). Scale bars = 100 μm in B; 1 mm in G (applies to D–G). [Color figure can be viewed at wileyonlinelibrary.com]

photomicrograph and the threshold image of FMRP staining. This pixel-based threshold analysis provides a readily, quantitative demonstration of the cells with high FMRP levels. A list of the most prominent FMRP-rich neuronal cell groups is summarized in Table 2. For naming individual neuronal cell groups, we adopt the nomenclature of the Allen Mouse Brain Atlas (http://atlas.brain-map.org). For identifying the rostral-caudal and the lateral-medial levels of the illustrated images, we compare our sections with the Mouse Brain Atlas (Paxinos and Franklin, 2013).

To further quantify the differential expression levels of FMRP among individual neuronal cell groups, we measured and compared the intensity of FMRP immunoreactivity in individual cell bodies in 85 selected neuronal cell groups (Fig. 15). At the cellular level, FMRP is most extensively localized in the cytoplasm of cell bodies. Labeled cell bodies vary greatly in size. It is a reasonable assumption that the majority of small cell bodies in the white matter are glial cells, while large cell bodies in the gray matter are mostly neuronal. In general, FMRP staining intensity is consistently low in the white matter. Our quantification and subsequent description focus on FMRP distribution pattern in the gray matter with respect to individual cell groups listed in the brain atlas. These cell groups are commonly called nuclei or neuronal cell groups, as they are generally identified based on packaging patterns of neuronal cell types. Within individual neuronal cell groups, we did not attempt to differentiate glial from neuronal cells. Our cellular quantification analyses include only labeled cell bodies with a cross-sectional cell body area larger than 40 μm^2, which excludes a large percentage of glial cells and, thus, preferentially represents neuronal population.

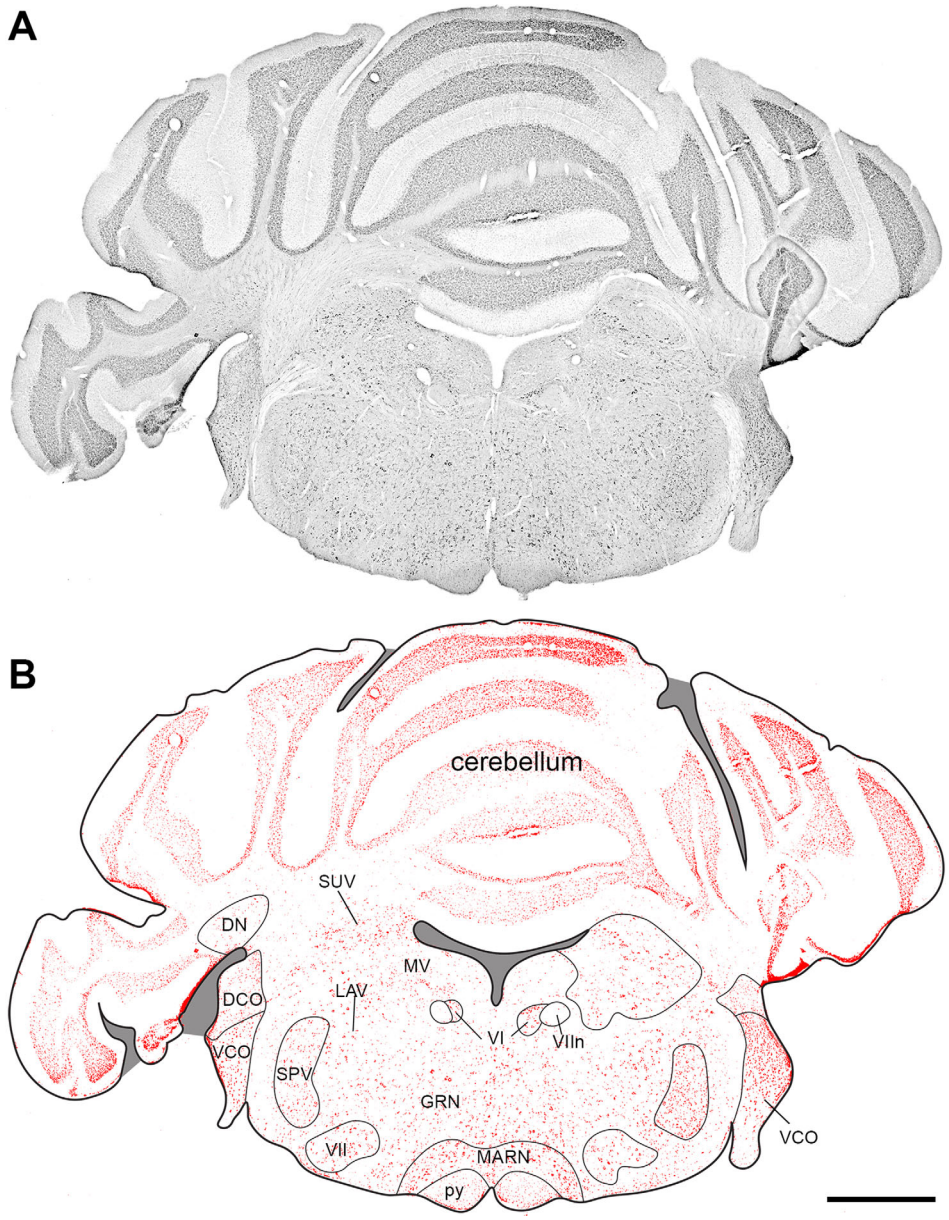

Figure 6. FMRP (7G1) immunostaining in the coronal plane at the level of the cerebellum and cochlear nuclei. **A**: The photomicrograph. **B**: The threshold image. Gray shades indicate the ventricle and areas without brain tissue. Scale bar = 1 mm. [Color figure can be viewed at wileyonlinelibrary.com]

In the following sections of the Results, we describe the distribution patterns of FMRP in each brain area and present high-magnification images of selected brain areas in Figures 16–27. It is worth noting that the distribution pattern of FMRP appears comparable across the six male mice of 5–6 weeks old examined in this study. Images illustrated in Figures 5–14 and 16–27 are from the same animal, while Figures 2–4 are from a different animal.

FMRP staining in the brainstem and spinal cord

Our samples include only the most rostral portion of the spinal cord containing C1–2 segments. In this portion, the spinal cord contains FMRP-rich cells of various sizes throughout the gray matter (Fig. 16A). Labeled cells were detected in both dorsal and ventral horns, indicating that both sensory and motor neurons contain FMRP. A group of large cells display particularly intense staining in the ventral horn (Fig. 16B, arrows), intermixing with cells with relatively lighter staining (Fig. 16B, arrowheads). The white matter of the spinal cord contains weakly labeled small cells, presumably glial cells (Fig. 16C, arrowheads).

In the caudal brainstem (Fig. 17), the inferior olive complex (IO), the magnocellular part of the lateral reticular nucleus (LRNm), the nucleus raphe pallidus and obscurus (RPA and RO), the external cuneate nucleus (ECU), and the dorsal motor nucleus of the vagus nerve (DMX) all stand out prominently, with a remarkably high

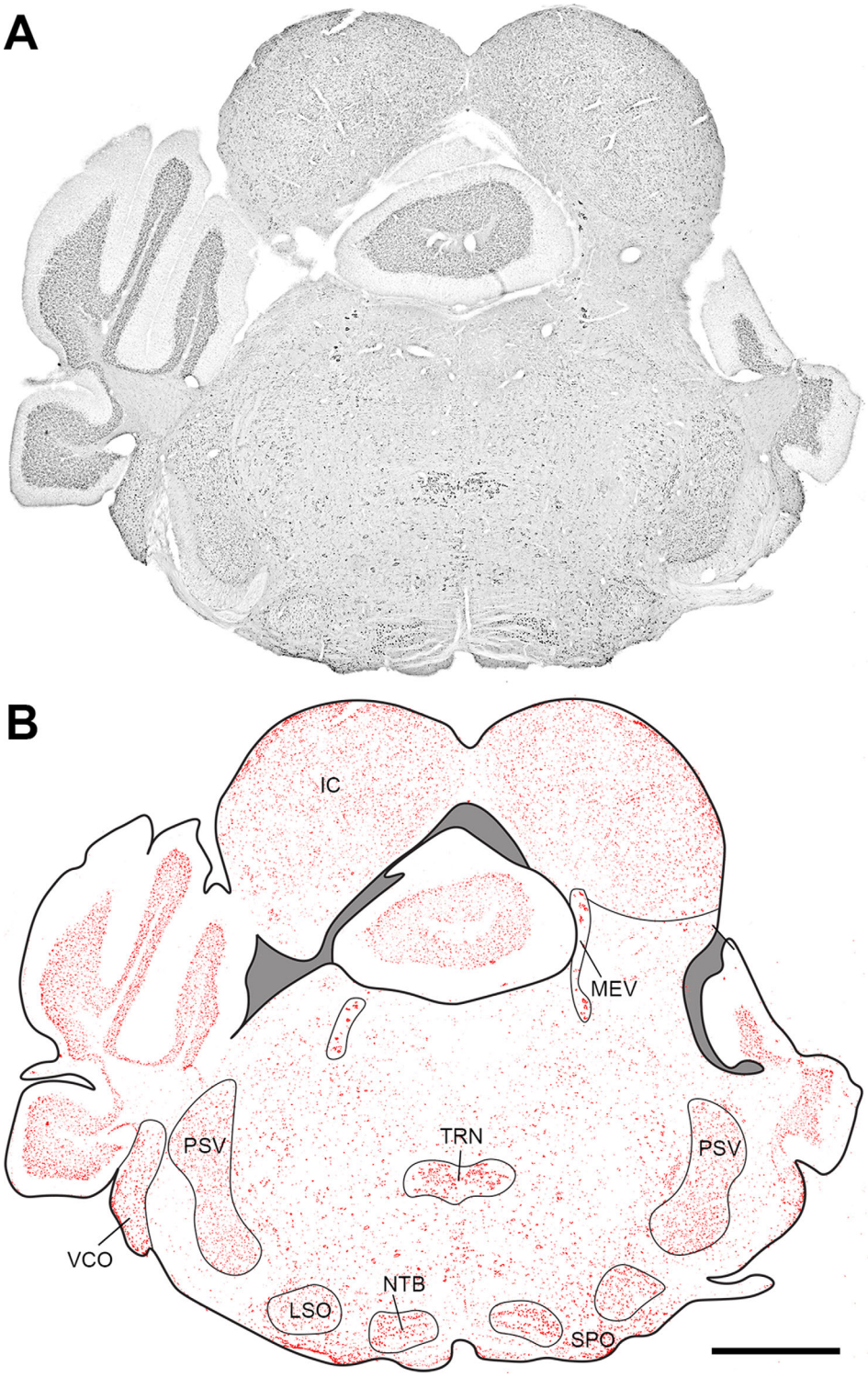

Figure 7. FMRP (7G1) immunostaining in the coronal plane at the level of the inferior colliculus. **A**: The photomicrograph. **B**: The threshold image. Gray shades indicate the ventricle and areas without brain tissue. Scale bar = 1 mm. [Color figure can be viewed at wileyonlinelibrary.com]

intensity of FMRP staining (Fig. 17A–I). Darkly labeled cells are also found in the gracile nucleus (GR), the cuneate nucleus (CU), the giganticellular reticular nucleus (GRN), the abducens nucleus (VI), the facial motor nucleus (VII), and the spinal nucleus of the trigeminal (SPV). The SPV contains several subdivisions with a wide span along the rostrocaudal dimension. FMRP-rich cells are detected throughout this complex, mixed with cells with relatively low intensities of FMRP immunoreactivity. Similarly, the reticular nucleus contain both darkly and weakly labeled cells. In contrast, most cells are weakly labeled in the hypoglossal nucleus (XII) and the nucleus of the solitary tract (NTS), which are immediately adjacent to DMX (Fig. 17J,K). Quantification

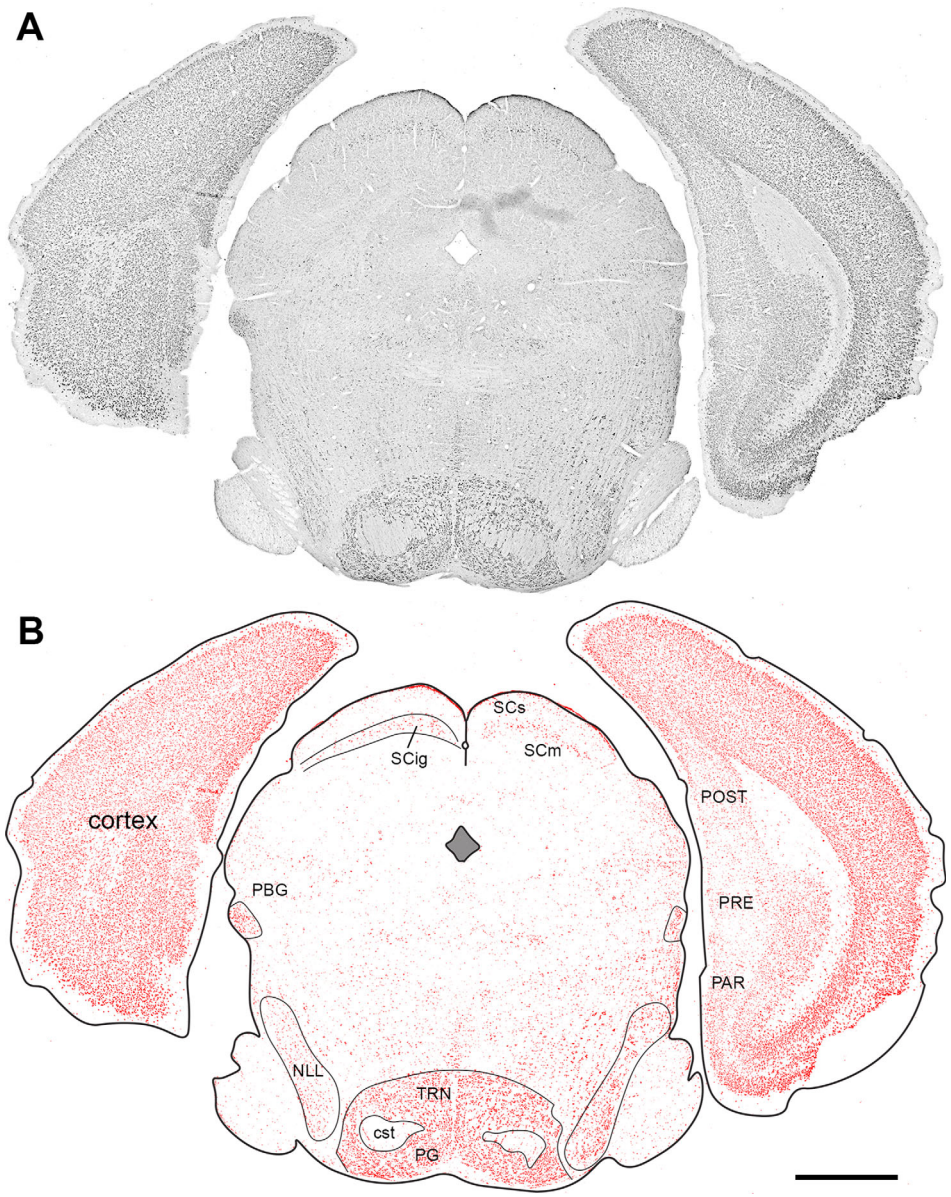

Figure 8. FMRP (7G1) immunostaining in the coronal plane at the level of the superior colliculus. **A**: The photomicrograph. **B**: The threshold image. Gray shade indicates the ventricle. Scale bar = 1 mm. [Color figure can be viewed at wileyonlinelibrary.com]

analysis confirms a significantly higher intensity of FMRP immunoreactivity in DMX than XII at the individual cell level ($P < 0.0001$; Fig. 15A).

At more rostral levels, where the vestibulocochlear nerve enters the brainstem (Fig. 18), auditory nuclei exhibit high levels of FMRP, including the dorsal and ventral portions of the cochlear nucleus (DCO and VCO; Fig. 18A), the superior olivary complex (SOC; Fig. 18E), the nucleus of the trapezoid body (NTB; Fig. 18E), and the nuclei of the lateral lemniscus (NLL; Fig. 18B). The two portions of the cochlear nucleus, DCO and VCO, exhibit different staining patterns. VCO contains distinct darkly labeled cell bodies throughout the nucleus, while cells in DCO are more closely packed and exhibit a wide range of FMRP staining intensity. The intensity of FMRP immunostaining is significantly higher in VCO than in DCO ($P < 0.0001$; Fig. 15A). A differential FMRP staining pattern is also seen between SOC and NTB. The staining intensity of NTB cells appears higher than that of the adjacent SOC nuclei including the lateral superior olive (LSO), the medial superior olive (MSO), and the superior paraolivary nucleus (SPO). This observation is confirmed with quantitative comparison between NTB and LSO ($P < 0.05$; Fig. 15A). Similarly, FMRP intensity in the vestibular nuclei is not uniform. The medial portion of the vestibular nucleus (MV) shows lower FMRP staining intensities than the lateral, superior and spinal portions (LAV, SUV, and SPIV; Fig. 18C,D). These differences are statistically significant ($P < 0.01$–0.0001; Fig. 15A).

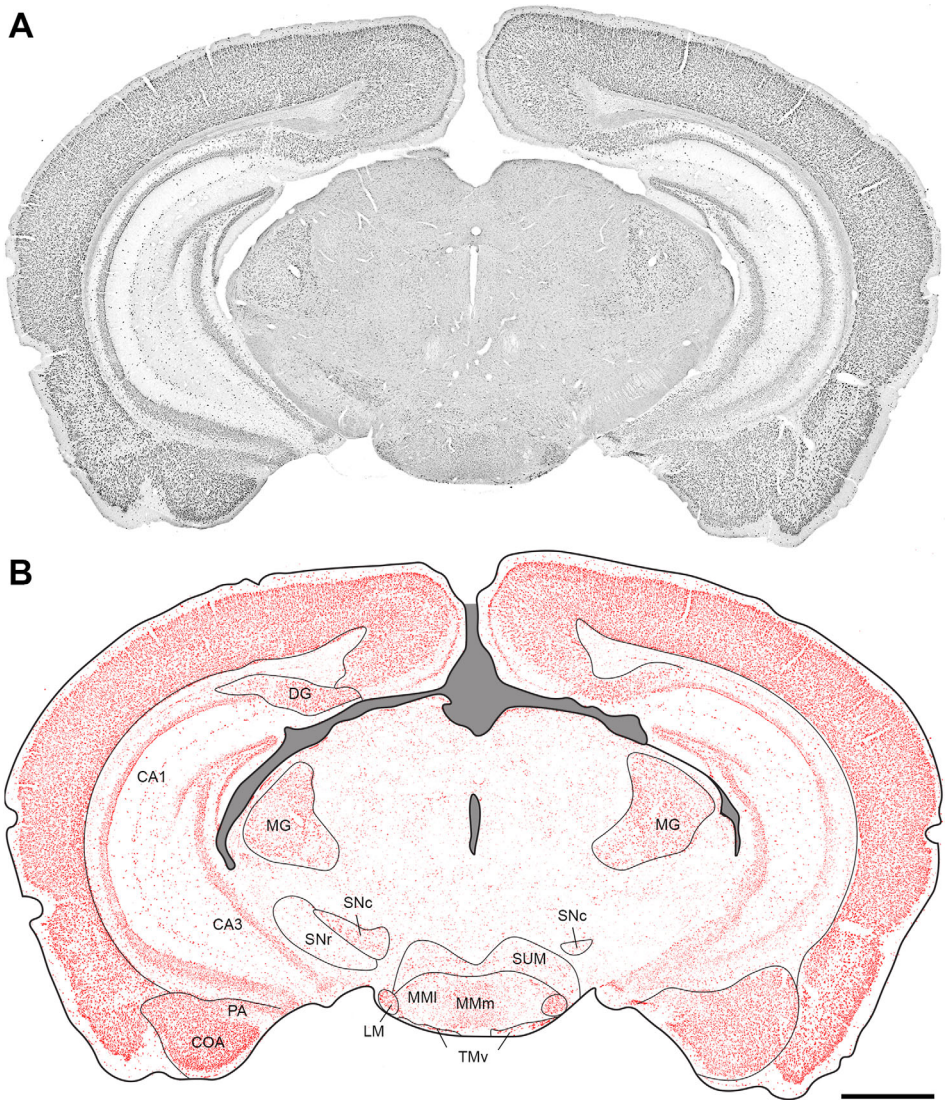

Figure 9. FMRP (7G1) immunostaining in the coronal plane at the level of the isocortex and caudal thalamus. **A**: The photomicrograph. **B**: The threshold image. Gray shades indicate the ventricle and areas without brain tissue. Scale bar = 1 mm. [Color figure can be viewed at wileyonlinelibrary.com]

The most rostral portion of the brainstem (Fig. 19) is largely occupied by the pontine reticular nucleus (PRN). PRN is low in FMRP immunostaining in general, although scattered neurons with strong labeling are also found (see Fig. 7). The tegmental reticular nucleus (TRN) and the pontine gray (PG) are heavily loaded with FMRP, in high contrast to the surrounding areas in the brainstem and midbrain (Fig. 19A). The principal sensory nucleus of the trigeminal (PSV) and the motor nucleus of trigeminal (V) also contain a high density of FMRP-rich cells (Fig. 19B). It is interesting to note a group of intensely stained cells embedded in the motor root of the trigeminal nerve. These cells are smaller and more darkly labeled than the cells in the adjacent motor nucleus of trigeminal (Figs. 15B, 19B).

FMRP staining in the midbrain

FMRP staining is generally low in the midbrain (Fig. 20). Nevertheless, a number of cell groups containing substantial FMRP immunoreactivity are detected. First, cells in both the external and central nuclei of the inferior colliculus (ICe and ICc) are darkly labeled, with comparable staining intensities (Fig. 15A, 20A–C). In contrast, cells in the adjacent periaqueductal gray (PAG) are weakly labeled (Fig. 20D). Second, the large cells of the midbrain trigeminal nucleus (MEV) show strong staining and are among the darkest cells for FMRP immunostaining in the entire brain (Figs. (15 and 20)D). Third, the intermediate gray layer of the superior colliculus (SCig) exhibit a uniquely strong staining for FMRP (Fig. 20E,F), as compared to other SC layers

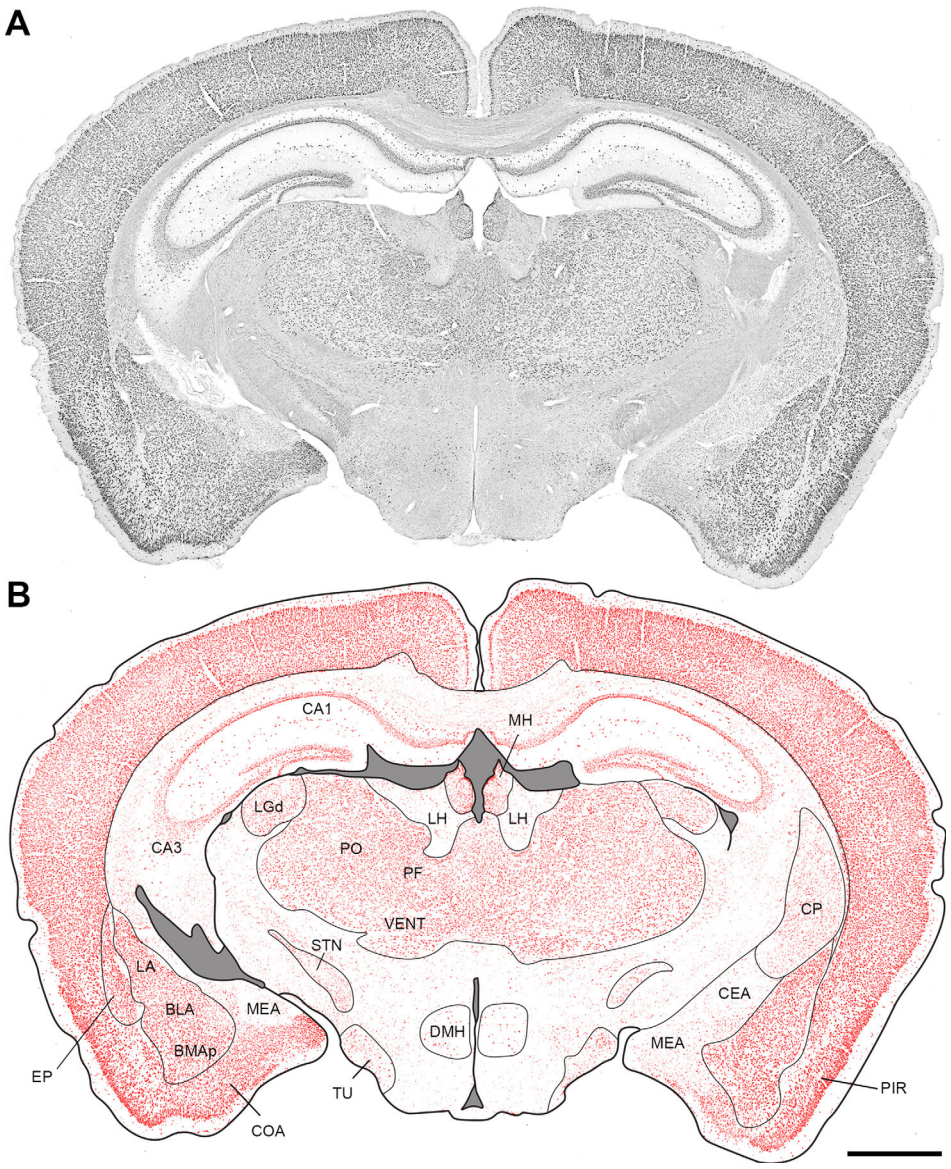

Figure 10. FMRP (7G1) immunostaining in the coronal plane at the level of the isocortex and middle thalamus. **A**: The photomicrograph. **B**: The threshold image. Gray shades indicate the ventricle and areas without brain tissue. Scale bar = 1 mm. [Color figure can be viewed at wileyonlinelibrary.com]

above and below ($P < 0.0001$; Fig. 15B). Fourth, most cells in the parabigeminal nucleus (PBG) exhibit distinctly high levels of FMRP immunostaining (Fig. 20G). FMRP intensity in PBG is significantly higher than that in SCig ($P < 0.0001$; Fig. 15B). Finally, darkly labeled cells are detected in the compact part of the substantia nigra (SNc; Fig. 19C) and the red nucleus (RN; Fig. 2).

FMRP staining in the thalamus

The entire thalamus displays high and relatively uniform levels of FMRP immunoreactivity (Fig. 21). Notably, differential FMRP intensities are detected in two thalamic areas. The first differential pattern is seen in the lateral geniculate complex (LG). The ventral LG division (LGv) and the intergeniculate leaflet (IGL) show significantly lower FMRP staining intensities than the dorsal LG division (LGd; Fig. 21A–C; $P < 0.001$–0.0001; Fig. 15D). The second differential pattern is seen in the epithalamus where the lateral habenula (LH) is stained notably lighter than the medial habenula (MH; Fig. 21D). However, cellular quantification reveals no significant difference in FMRP intensity of individual cell bodies between MH and LH ($P = 0.10$; Fig. 15D), indicating that the stronger staining in MH is primarily due to a higher cell density in MH rather than higher FMRP intensities of individual cell bodies (Fig. 21E,F). Nonetheless, FMRP intensity in both MH and LH are significantly lower than that in the ventrally located parafasciular nucleus (PF; $P < 0.001$; Figs. 15D, 21D).

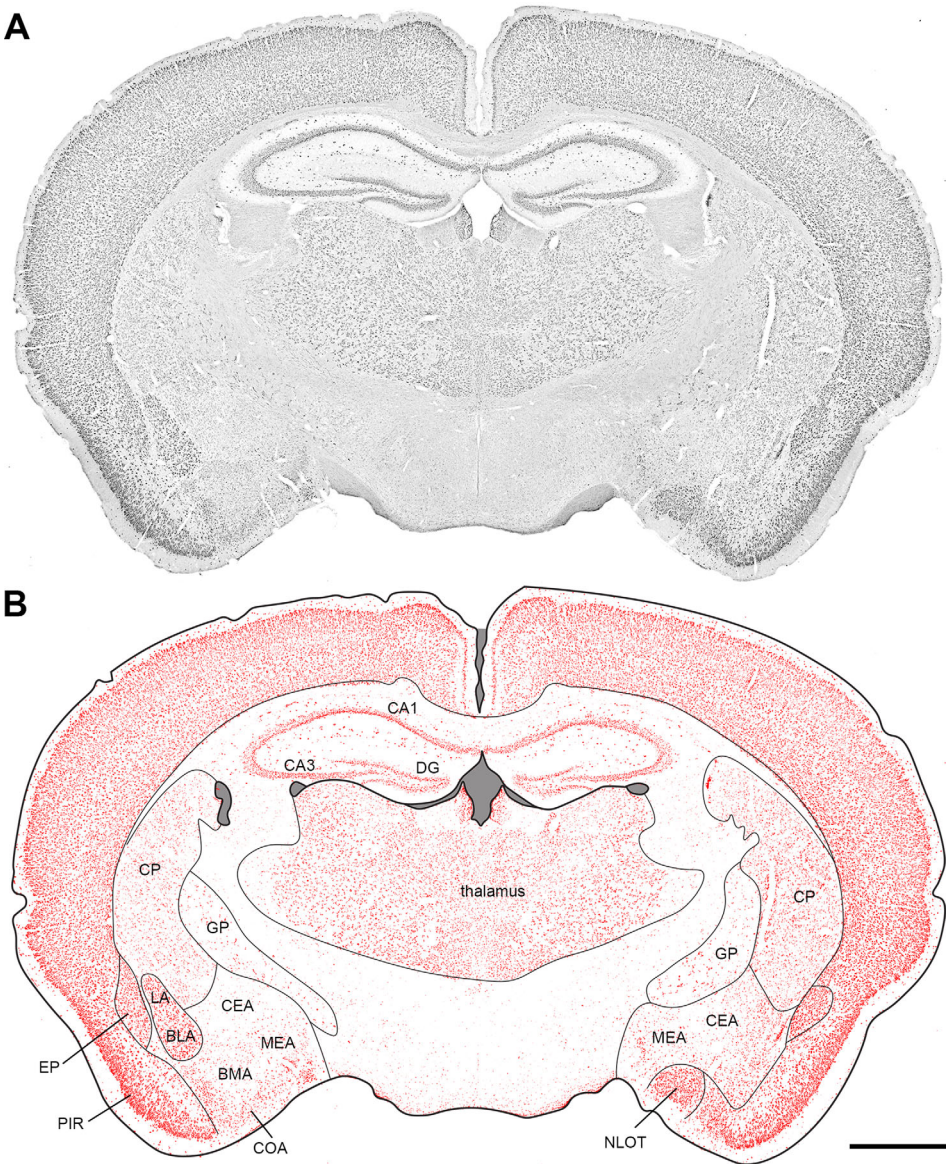

Figure 11. FMRP (7G1) immunostaining in the coronal plane at the level of the isocortex and rostral thalamus. **A**: The photomicrograph. **B**: The threshold image. Gray shades indicate the ventricle and areas without brain tissue. Scale bar = 1 mm. [Color figure can be viewed at wileyonlinelibrary.com]

FMRP staining in the hypothalamus

In contrast to the adjacent thalamus, most of the hypothalamus exhibits strikingly lower FMRP intensity (Fig. 22). A number of cell groups in the mammillary body, however, show strong FMRP immunostaining, including the lateral mammillary nucleus (LM; Fig. 22A), the ventral part of the tuberomammillary nucleus (TMv; Fig. 22B), and the medial part of the medial mammillary nucleus (MMm; Fig. 22D). In contrast, FMRP staining is weak in the adjacent ventral premammillary nucleus (PMv; Fig. 22F). Additional hypothalamic nuclei containing darkly labeled cells for FMRP are the dorsomedial nucleus of the hypothalamus (DMH, Fig. 22C), the tuberal nucleus (TU; Fig. 22E), the parasubthalamic nucleus (PSTN, Fig. 22G), and the subthalamic nucleus (STN; Fig. 22H).

FMRP staining in the cerebellum

Purkinje neurons at the interface between the granular and the molecular layers of the cerebellum have been reported as one of the neuronal cell types that are most reactive to FMRP immunocytochemistry (Devys et al., 1993). Here we show the average staining intensity within the cell bodies of the Purkinje neurons is medium to strong (Figs. 15B, 23A). Prominent staining is also seen in the granular layer, which consists of small neurons, while in the molecular layer only few cells show strong labeling. Cells in the three cerebellar

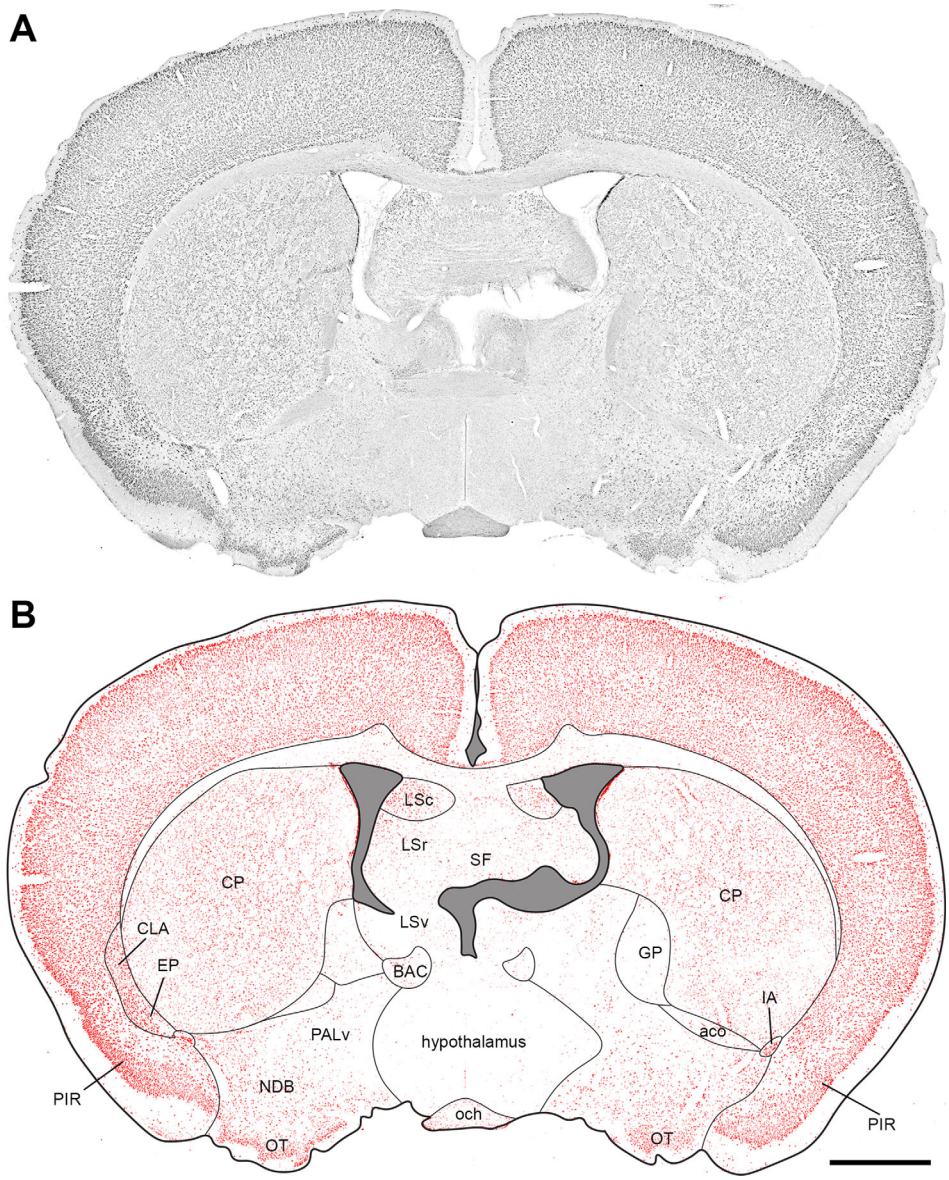

Figure 12. FMRP (7G1) immunostaining in the coronal plane at the level of the caudal striatum. **A**: The photomicrograph. **B**: The threshold image. Gray shades indicate the ventricle and areas without brain tissue. Scale bar = 1 mm. [Color figure can be viewed at wileyonlinelibrary.com]

nuclei, the fastigial nucleus (FN), interposed nucleus (IP), and dentate nucleus (DN) are stained strongly at comparable levels (Figs. 15B, 23B).

FMRP staining in the cerebral cortex: isocortex

Throughout the entire isocortex, intense FMRP staining is seen in almost all areas and in every layer (Fig. 24). Careful examination with high-power images, however, reveals heterogeneous internal patterns of FMRP distribution within specific isocortex areas. For example, in the rostral portion of the primary somatosensory cortex, small granular cells in layer 4 exhibit notably lower FMRP intensities as compared to other layers, while cells in layers 2–3 appear more darkly labeled than other layers (Fig. 24A). A more dramatic pattern of low FMRP intensities of layer 4 granular cells is seen in the retrosplenial area, in particular its ventral part (RSPv, called the area 29) (Fig. 24B). In contrast, cells in layer 4 of the visual area exhibit similar levels of staining as compared to other layers of the same area (Fig. 24C). As another example of heterogeneous FMRP distribution in the isocortex, a unique group of neurons with particularly intense FMRP staining are found in the anterior cingulate area (ACA; Fig. 24D). These cells span layers 2/3 and 5 but are not usually found in layer 6. These cells are among the most darkly stained cells in the entire brain. At the level of caudal cortex, it is also noted that FMRP staining intensity is generally

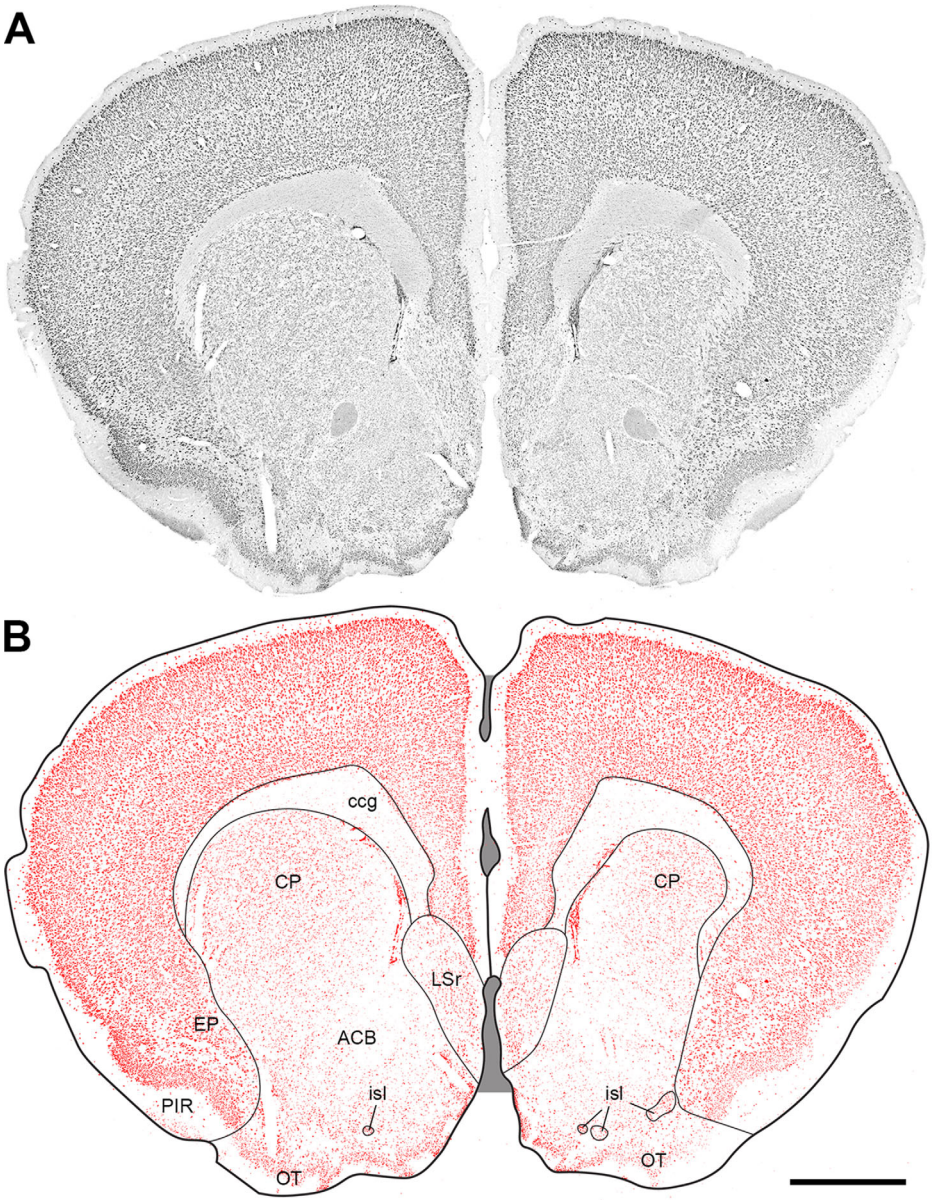

Figure 13. FMRP (7G1) immunostaining in the coronal plane at the level of the rostral striatum. **A**: The photomicrograph. **B**: The threshold image. Gray shades indicate the ventricle and areas without brain tissue. Scale bar = 1 mm. [Color figure can be viewed at wileyonlinelibrary.com]

lower in the parasubiculum (PAR), postsubiculum (POST), and presubiculum (PRE) than other cortical areas (Fig. 8).

We quantified FMRP intensity at the individual neuron level in four isocortical areas using one-way ANOVA followed with Tukey's test for multiple comparisons (Fig. 15C). The intensities of FMRP immunoreactivity are significantly different between layers within each cortical area ($P < 0.0001$). Subsequent comparisons further reveal that layer 4 in area 29 of the retrosplenial area has significantly lower intensity in FMRP than any other layers ($P < 0.0001$). In addition, FMRP intensity in layer 6a is significantly lower than the adjacent layers 5 and 6b ($P < 0.01$–0.0001). In the primary visual cortex, cells in layers 1 and 6b have significantly higher FMRP intensities than other layers ($P < 0.0001$). As expected, layer 4 of the primary somatosensory cortex at the level of the major body of the caudoputamen shows significantly lower FMRP intensity than layers 1, 2/3, and 5 ($P < 0.0001$), but not layers 6a and 6b. Similar to the somatosensory area, the anterior cingulate area (ACA) shows lower FMRP staining in deep layers 5 and 6 than the more superficial layers 1–3. As expected, FMRP intensity of the darkly labeled cells (DN in Fig. 15C) spanning layers 2–5 is significantly higher than any other layers of this cortical region ($P < 0.01$–0.0001).

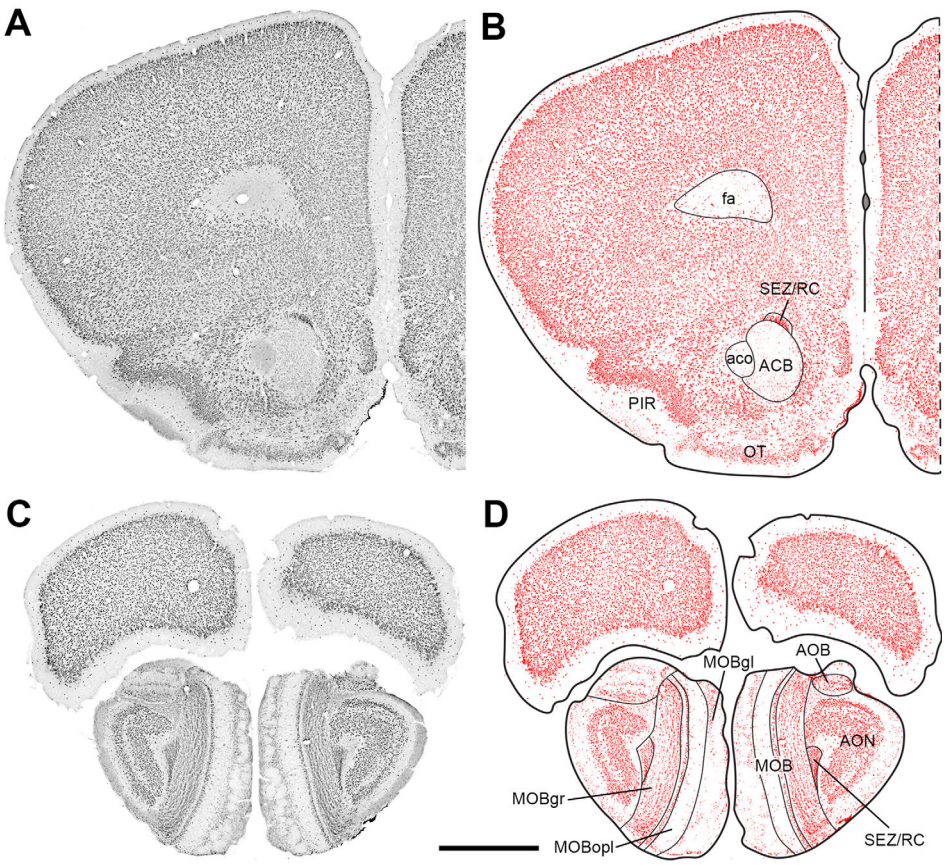

Figure 14. FMRP (7G1) immunostaining in the coronal plane at the level of the rostral cortex (**A,B**) and olfactory bulb (**C,D**). A,C: The photomicrographs. B,D: The threshold images. Scale bar = 1 mm. [Color figure can be viewed at wileyonlinelibrary.com]

FMRP staining in the cerebral cortex: cortical subplate

The cortical subplate contains the cell groups in the ventral and adjacent medial to the cortical isocortex, including the claustrum (CLA), the endopiriform nucleus (EP), and several amygdalar nuclei. FMRP immunostaining is strong in most of these cell groups except in the posterior amygdalar nucleus (PA) and the anterior portion of the basomedial amygdalar nucleus (BMAa; Fig. 25). Cellular quantification confirms that FMRP intensity in PA is significantly lower than the adjacent basolateral amygdalar nucleus (BLA; $P < 0.0001$; Fig. 15B) and FMRP intensity in BMAa is significantly lower than the posterior BMA (BMAp; $P < 0.0001$; Fig. 15B).

FMRP staining in the cerebral cortex: hippocampus and olfactory bulb

In all regions of the hippocampus, the pyramidal layer of CA1–3 and the granule cell layer of the dentate gyrus exhibit strong FMRP staining (Fig. 26). In particular in CA1, FMRP immunoreactivity accumulates intensively in the ventral portion of the pyramidal cell bodies, giving rise to a dark line in FMRP staining at the interface of the pyramidal layer and the stratum radiatum layer (Fig. 26A). This dark line is not seen in other regions of the hippocampus including CA3 and the dentate gyrus (Fig. 26B,C). FMRP can also be detected in the proximate portion of the dendrites extending from the CA1 pyramidal layer (arrows in Fig. 26A). In addition, darkly labeled cells were found scattered in other layers of the hippocampus, including the stratum oriens and radiatum layers of CA1–3, as well as the molecular and polymorph layers of the dentate gyrus (Fig. 26A–C).

All portions of the olfactory area are rich in FMRP immunoreactivity, including the main olfactory bulb (MOB), the accessory olfactory bulb (AOB), the anterior olfactory nucleus (AON), the piriform area (PIR), the cortical amygdalar area (COA), and the nucleus of the lateral olfactory tract (NLOT; Fig. 14C,D). Within the MOB, the staining intensity of the cell bodies is lower in the glomerular layer than the mitral layer (Figs. 15D, 26D).

FMRP staining in the cerebral nuclei: striatum and pallidum

The cortical nuclei contain two major groups, the striatum and pallidum. Most cells in the two groups contain FMRP immunoreactivity at low to medium levels.

TABLE 2.
FMRP-Rich Neuronal Cell Groups in the Mouse Brain

Neuronal cell groups	Neuronal cell groups	Neuronal cell groups
Spinal Cord	**Cerebellum**	**Cerebral Cortex**
Gray matter	Dentate nucleus (DN)	Isocortex – all areas
	Fastigial nucleus (FN)	Basolateral amygdalar nucleus (BLA)
Brainstem	Interposed nucleus (IP)	Basomedial amygdalar nucleus,
Abducens nucleus (VI)	Granular cells	posterior part (BMAp)
Dorsal motor nucleus	Purkinje neurons	Claustrum (CLA)
of the vagus nerve (DMX)		Cortical amygdalar area (COA)
External cuneate nucleus (ECU)	**Midbrain**	Endopiriform nucleus (EP)
Facial motor nucleus (VII)	Inferior colliculus (IC)	Lateral amygdalar nucleus (LA)
Gigantocellular reticular nucleus (GRN)	Midbrain trigeminal nucleus (MEV)	
Gracile nucleus (GR)	Parabigeminal nucleus (PBG)	**Cerebral Nuclei**
Inferior olivary complex (IO)	Red nucleus (RN)	Caudoputamen (CP)
Lateral reticular nucleus,	Substantia nigra, compact part (SNc)	Diagonal band nucleus (NDB)
magnocellular part (LRNm)	Superior colliculus, intermediate gray layer (SCig)	Globus pallidus (GP)
Motor nucleus of the trigeminal (V)		Intercalated amygdalar nucleus (IA)
motor root of the trigeminal nerve (moV)	**Thalamus**	Islands of Calleja (isl)
Nucleus of the lateral lemniscus (NLL)	Lateral geniculate complex, dorsal part (LGd)	Medial amygdalar nucleus,
Nucleus of the trapezoid body (NTB)	Lateral habenula (LH)	posteroventral part (MEApv)
Nucleus raphe obscurus (RO)	Lateral posterior nucleus of the thalamus (LP)	Olfactory tubercle (OT)
Nucleus raphe pallidus (RPA)	Medial geniculate complex (MG)	
Pontine gray (PG)	Medial habenula (MH)	**Hippocampus**
Principal sensory nucleus	Parafascicular nucleus (PF)	Dentate gyrus (DG)
of the trigeminal (PSV)	Posterior complex of the thalamus (PO)	Field CA1 (CA1)
Spinal nucleus of the trigeminal (SPV)	Ventral group of the dorsal thalamus (VENT)	Field CA2 (CA2)
Superior olivary complex (SOC)	Ventral posterior complex of the thalamus (VP)	Field CA3 (CA3)
Lateral superior olive (LSO)[1]		
Medial superior olive (MSO)[1]	**Hypothalamus**	**Olfactory**
Superior paraolivary nucleus (SPO)[1]	Dorsomedial nucleus of the hypothalamus (DMH)	Accessory olfactory bulb (AOB)
Tegmental reticular nucleus (TRN)	Lateral mammillary nucleus (LM)	Anterior olfactory nucleus (AON)
Ventral cochlear nucleus (VCO)	Medial mammillary nucleus, medial part (MMm)[1]	Main olfactory bulb (MOB)
Vestibular nuclei (VNC)	Parasubthalamic nucleus (PSTN)	glomerular layer (MOBgl)
Lateral vestibular nucleus (LAV)	Subthalamic nucleus (STN)	granule layer (MOBgr)
Spinal vestibular nucleus (SPIV)	Tuberal nucleus (TU)	mitral layer (MOBmi)
Superior vestibular nucleus (SUV)	Tuberomammilliary nucleus, ventral part (TMv)	Nucleus of the lateral olfactory tract (NLOT)

[1]The cell groups whose name is not included in the Allen Mouse Brain Atlas (http://atlas.brain-map.org).

The caudoputamen (CP), the largest striatum cell group, is clearly less stained than the adjacent isocortex and the cell groups in the cortical subplate (Figs. 15B, 25E–G, 27A,B). Nonetheless, cells are more darkly stained in CP in general than the nucleus accumbens (ACB) and the fundus of striatum. Within the lateral septal complex, the caudodorsal part of the lateral septal nucleus (LSc) exhibits notably higher FMRP intensities than other cell groups of the complex (see Fig. 11). Among the striatum-like amygdalar nuclei, the central and medial amygdalar nuclei (CEA and MEA) exhibit low levels of staining, while the intercalated amygdalar nucleus (IA) contains prominent FMRP staining (Figs. 25D–G, 27F). All layers of the olfactory tubercle (OT) are rich in FMRP immunoreactivity, including the embedded islands of Calleja (Figs. 12–14, 1997C). In the pallidum, the most prominent FMRP-rich cells are found in the globus pallidus (GP) and the diagonal band nucleus (NDB; Fig. 27D,E).

DISCUSSION

In this study we provide a systematic map of the cellular distribution of the fragile X mental retardation protein (FMRP) throughout the mammalian brain. We show that the FMRP expression level is highly differential among individual neuronal cell groups in young mature brains. This finding leads to important implications regarding FMRP function in normal brains and may shed light on understanding the pathology of the fragile X syndrome (FXS).

Differential expression of FMRP in young mature brains

There are two current notions regarding the expression pattern of FMRP in the mammalian brain. The first notion is that FMRP expression is high in some brain areas and low in other regions (Abitbol et al., 1993; Devys et al., 1993; Hinds et al., 1993; Khandjian et al., 1995; Verheij et al., 1995). This "regional distribution"

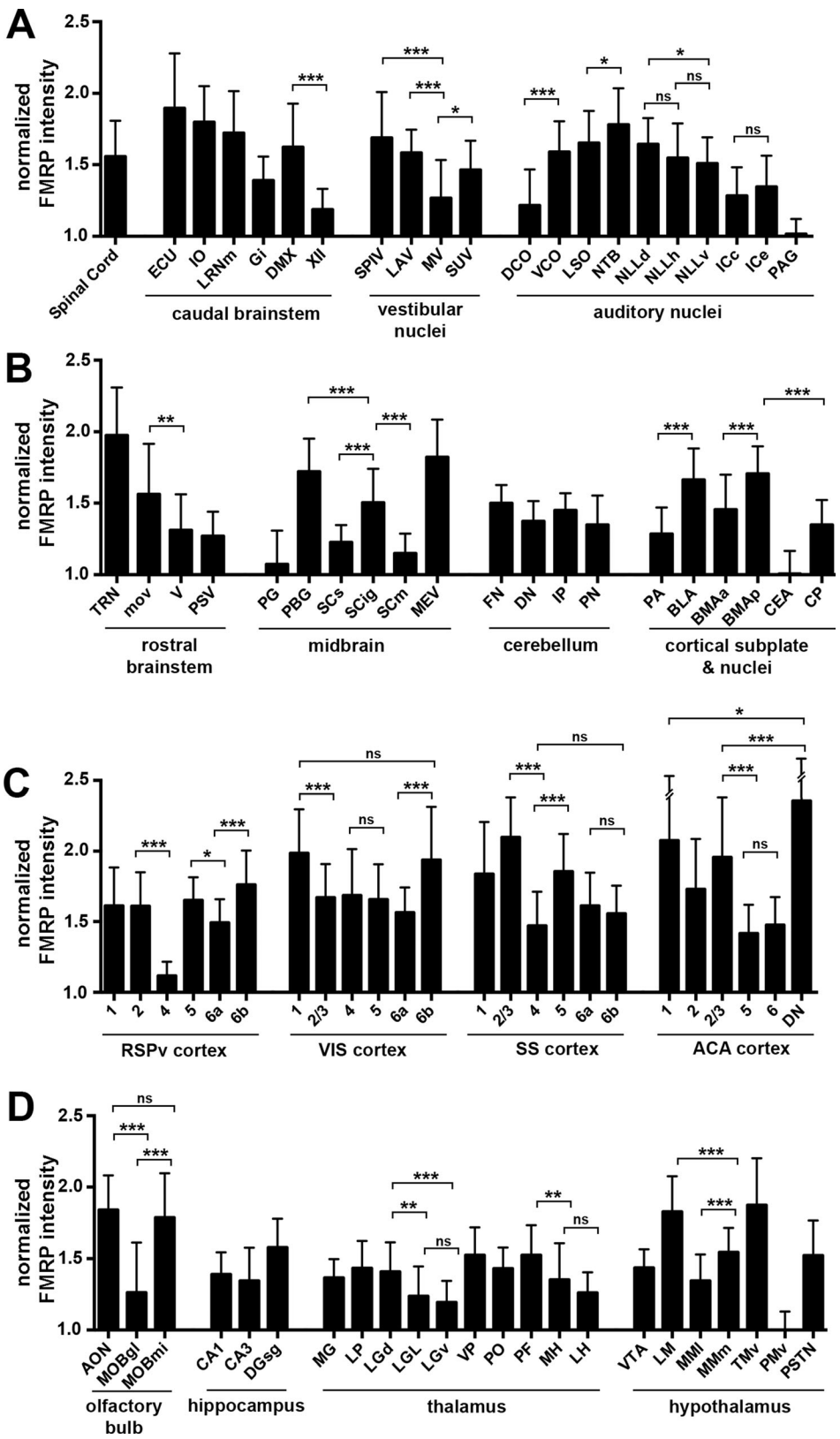

Figure 15. Cellular quantification of FMRP intensity in selected neuronal cell groups. **A**: The spinal cord and cell groups in the caudal brainstem and vestibular and auditory nuclei. **B**: Cell groups in the rostral brainstem, midbrain, cerebellum, as well as the cortical subplate and nuclei. **C**: Layers of isocortical areas. **D**: Cell groups in the olfactory bulb, hippocampus, thalamus, and hypothalamus. FMRP intensities were normalized as described in the Materials and Methods. Higher intensities indicate higher levels of FMRP staining at the individual cell level. For each cell group, 30 neurons were measured and averaged. Measurements for each cortical area were taken at levels comparable to Fig. 24. Error bars are SD. $*P < 0.01$. $**P < 0.001$. $***P < 0.0001$. "ns," not significant.

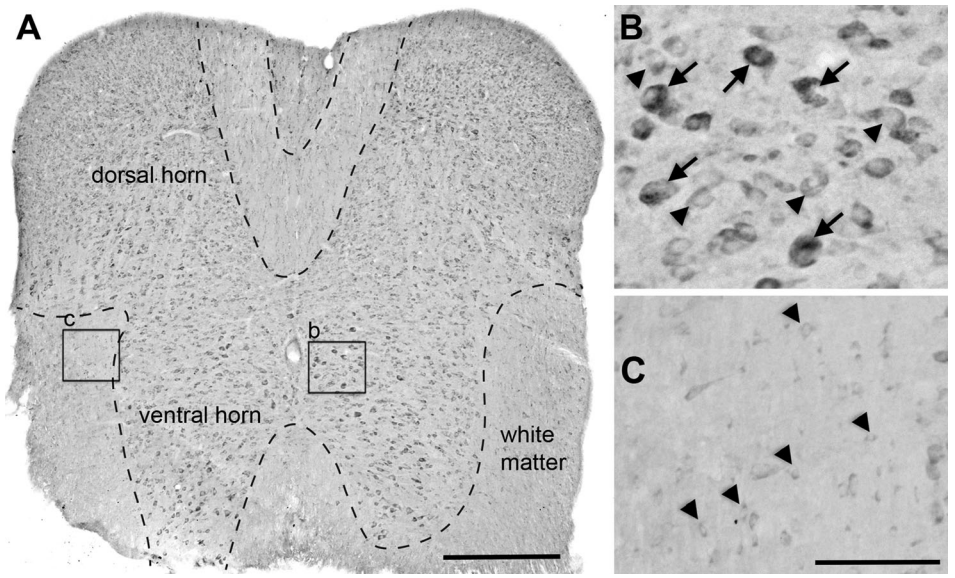

Figure 16. High-magnification images of FMRP (7G1) immunostaining in the spinal cord. **A**: The spinal cord at the approximate level of C-2 segment. Closer looks of the boxes are displayed in B,C. Dashed lines indicate the borders between the white and gray matters. **B**: The gray matter contains darkly (arrows) and relatively lightly (arrowheads) stained cells. **C**: The white matter contains small immunoreactive cell bodies (arrowheads), presumably glial cells. Scale bars = 500 μm in A; 100 μm in C (applies to B,C).

pattern has led to extensive studies of FMRP function in brain regions with high overall FMRP levels, such as the hippocampus and cortex. The second notion considers FMRP expression at the individual cell level and emphasizes that many neuronal types throughout the brain are as intensely stained for FMRP as the neurons in the hippocampus and cortex (Feng et al., 1997; Christie et al., 2009). This "universal distribution" concept argues that strong FMRP signals in some brain regions such as the hippocampus may be related to neuron size and density. This notion is supported by accumulating evidence of altered neuronal structure and function throughout the brain following FMRP loss or reduction, including the brainstem (Brown and Kaczmarek, 2011; Rotschafer et al., 2015) and thalamus (Kogan et al., 2004a).

Using systematic mapping of FMRP immunoreactivity in the entire brain and quantitative analyses at the individual cell level, the current study confirms the widespread distribution of FMRP-rich cells throughout the mammalian brain. More important, this study demonstrates a highly differential pattern of FMRP expression with regard to individual neuronal cell groups. In almost all major brain areas from the brainstem and midbrain to the thalamus and forebrain, cell groups high in FMRP expression are found to be located adjacent to cell groups low in FMRP expression. One of the most striking examples is that the FMRP expression level can differ notably between layers of the same cortical areas and between adjacent cortical areas of the same layers. The overall strong FMRP signal seen in the cortex and hippocampus is partially due to relatively higher percentages of neurons (and probably large glial cells) rich in FMRP in these areas than in other brain regions, in addition to the size and density of general neuronal population, as suggested by Feng et al. (1997).

It is interesting to speculate about the relationship of FMRP expression with other cellular properties of mature neurons. Clearly, the FMRP expression level of a neuron is not simply related to its general function. In the spinal cord and brainstem, both sensory and motor neurons contain high levels of FMRP. Equally important, not all nuclei involved in sensory processing and motor control express high levels of FMRP (see more discussion below). Consistently, sensory neurons in the thalamus express comparable levels of FMRP to most cortical and hippocampal neurons for cognitive and memory processing. In particular, two nuclei located adjacent to each other and involved in similar functional operations can vary dramatically in the level and pattern of FMRP expression. Examples include the dorsal and ventral portions of the cochlear nucleus, the primary targets of auditory nerve from the inner ear (Brown and Ledwith, 1990), as well as the anterior and posterior portions of the basomedial amygdalar nucleus, which both are a part of the fear response pathway (Rosen, 2004).

FMRP expression is also not specific to the type of neurotransmitters a neuron releases or to the

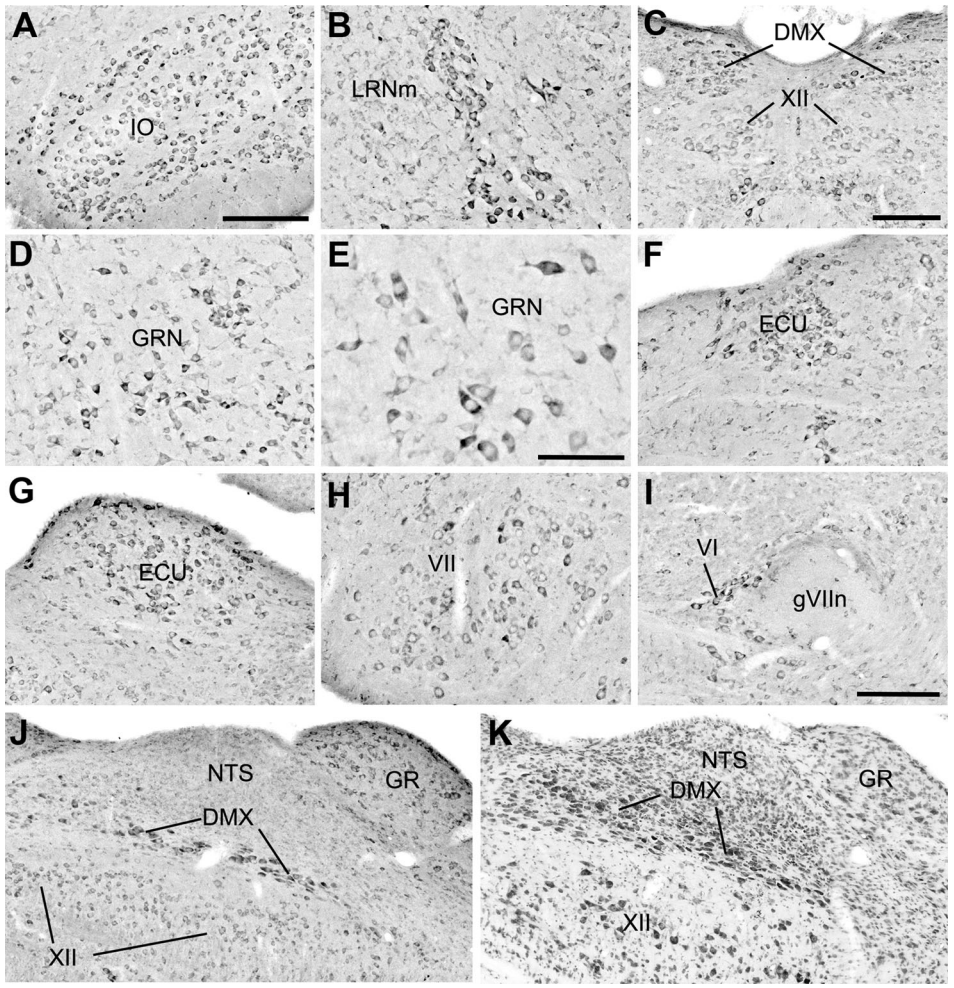

Figure 17. High-magnification images of FMRP (7G1) immunostaining in the caudal brainstem. **A,B**: High FMRP levels in the inferior olive complex (IO; A) and the magnocellular part of the lateral reticular nucleus (LRNm; B). **C**: The dorsal motor nucleus of the vagus nerve (DMX) exhibits stronger FMRP staining than the adjacent hypoglossal nucleus (XII). These two nuclei are also illustrated in J and K. **D,E**: The giganticellular reticular nucleus (GRN) contains darkly labeled neurons. E is at a higher magnification than D. **F,G**: The external cuneate nucleus (ECU) is rich in FMRP at both the rostral (F) and caudal (G) levels. **H,I**: FMRP immunoreactive neurons in the facial motor nucleus (VII; H) and the abducens nucleus (VI; I). **J,K**: 7G1 immunostaining (J) and the Nissl stain (K) on the adjacent sections containing DMX and XII. Note the relatively lower level of FMRP in XII as compared to the DMX. A–I are coronal sections while J–K are sagittal sections. Scale bar = 200 μm for A (applies to B,D,F–H,J,K); 200 μm for C,I; 100 μm in E.

expression of a number of biomarkers that characterize specialized neuronal cell types. For example, FMRP level is comparably high in principle neurons of the medial nucleus of the trapezoid body that release glycine (Bledsoe et al., 1990), hippocampal pyramidal neurons that use glutamate as a neurotransmitter (Deng et al., 2013), and GABAergic Purkinje neurons in the cerebellum (Saito et al., 1974). Similarly, nearly all neurons in the inferior olive strongly express both FMRP and calbindin (Yu et al., 2014), while the cerebellar molecular layer contains numerously darkly labeled small granular cells for FMRP, mostly known to be calbindin-negative (Schwaller et al., 2002). This broad overlap of FMRP expression with neuronal function and other cellular properties, along with the differential pattern of FMRP between individual cell groups, highlight the importance of FMRP signal in a wide range, but highly selected, brain activities. Exploring the underlying mechanisms of this selection is an important avenue for future investigations and is expected to dramatically enhance our understanding of FMRP regulation in the brain.

Implications related to FMRP function and FXS pathology

If a cell is normally rich in FMRP, it suggests an increased susceptibility of cell structure and function to the loss or reduction of this protein, as compared to

other cells that do not express the protein or require lower levels of FMRP for healthy function. It is important to note that the distribution pattern of FMRP described here is in young mature brains of 5–6-week-old mice. Although FMRP expression in the brain begins early in development and continues throughout life (Hinds et al., 1993), the FMRP level appears to be associated with specific developmental events (Tessier and Broadie, 2008; Cook et al., 2011; Gholizadeh et al., 2015). Special care should be taken when attempting to associate the distribution pattern of FMRP in mature brains to structural, physiological, and behavioral abnormalities found in FXS patients and FMR1 knockout animals. These abnormalities are accumulated consequences of constitutive FMRP reduction during the entire development as well as the acute influence of insufficient FMRP regulation after maturity. Furthermore, FMRP has been proposed to play distinct functions at specific developmental stages, from regulating neuronal differentiation during early development, mediating dendritic and synaptic pruning later in development, and to controlling activity-dependent neuronal plasticity after maturity (Till, 2010; Telias et al., 2013; Chaudhury et al., 2016). Characterization of FMRP cellular distribution patterns at critical developmental stages is essential for exploring specific contributions of various FMRP regulatory mechanisms to normal brain function. Below we discuss how FMRP expression levels in mature brains might be associated with physiological and behavioral outcomes in FXS patients and animals, with an emphasis on activity-dependent neuronal plasticity. This discussion is focused on three brain areas of high interest.

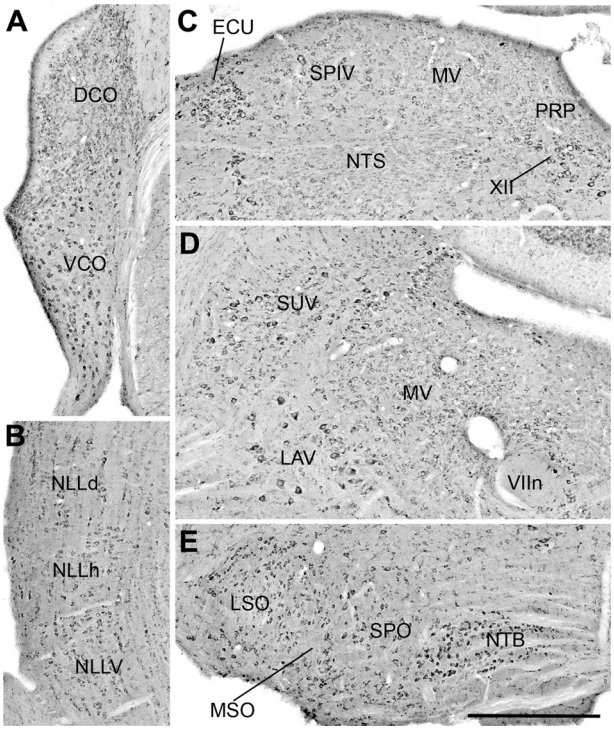

Figure 18. High-magnification images of FMRP (7G1) immunostaining in the vestibular and auditory brainstem nuclei. **A**: FMRP staining in the dorsal and ventral cochlear nuclei (DCO and VCO). **B**: FMRP staining in the three subnuclei of the nucleus of the lateral lemniscus (NLLd, NLLh, and NLLV). **C,D**: FMRP staining in the medial, spinal, lateral, and superior portions of the vestibular nucleus (MV, SPIV, LAV, and SUV). D was taken from a section more rostral than C. **E**: FMRP staining in the superior olive complex and the nucleus of the trapezoid body (NTB). Scale bar = 500 μm.

Subcortical sensory processing

Sensory information processing has recently received an increasing amount of attention in studying FXS pathology in humans and animal models (Sinclair et al., 2016). Abnormal sensory processing is common not only to individuals with FXS but also to autism spectrum disorders in general. One novel finding of our report is the identification of a large number of cell

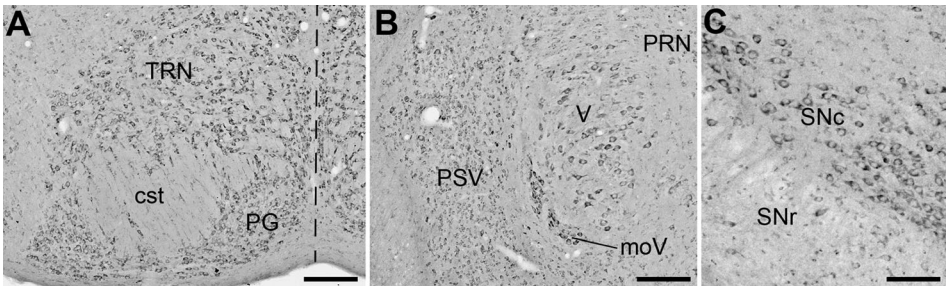

Figure 19. High-magnification images of FMRP (7G1) immunostaining in the rostral brainstem. **A**: Intense FMRP staining in the tegmental reticular nucleus (TRN) and the pontine gray (PG). Dashed line indicates the midline. **B**: FMRP staining in the principal sensory nucleus of the trigeminal (PSV) and the motor nucleus of the trigeminal (V). Note particularly high FMRP levels in neurons embedded in the motor root of the trigeminal nerve (moV). **C**: FMRP immunoreactive neurons in the compact pact of the substantia nigra (SNc). Scale bars = 200 μm in A,B; 100 μm in C.

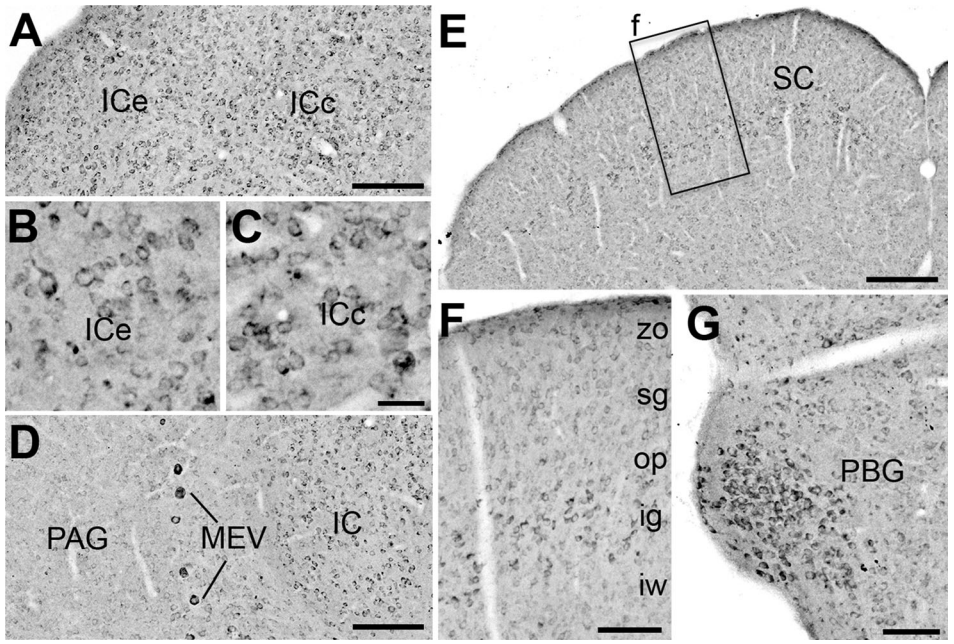

Figure 20. High-magnification images of FMRP (7G1) immunostaining in midbrain cell groups. **A–C**: FMRP immunoreactivity in the external and central nuclei of the inferior colliculus (ICe and ICc). B,C: At a higher magnification than A. **D**: FMRP staining is weak in the adjacent periaqueductal gray (PAG). Note darkly labeled neurons in the midbrain trigeminal nucleus (MEV). **E,F**: Intense FMRP staining in the intermediate gray layer (ig), but not other layers, of the superior colliculus (SC). F is a closer look of the box in E. **G**: Neurons in the parabigeminal nucleus are darkly labeled for FMRP immunocytochemistry. Scale bars = 250 μm in A,D,E; 50 μm in C (applies to B,C); 100 μm in F,G.

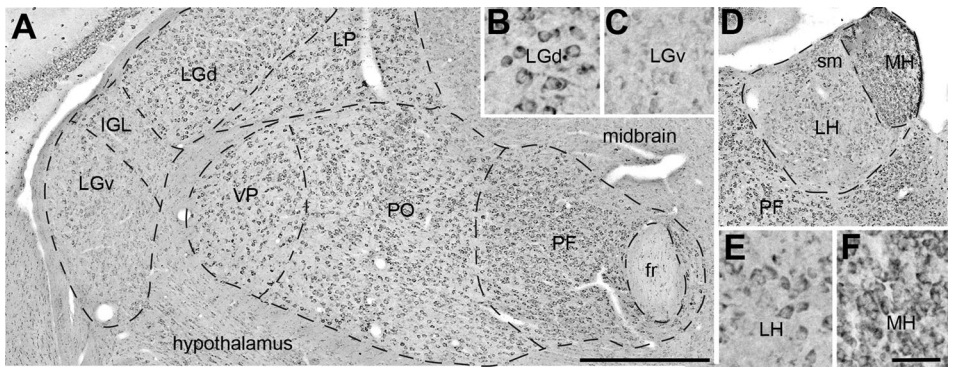

Figure 21. High-magnification images of FMRP (7G1) immunostaining in the thalamus. **A**: Strong FMRP staining in most thalamic cell groups but not the ventral portion of the lateral geniculate complex (LGv) and the intergeniculate leaflet (IGL). **B,C**: Closer looks of the neurons in the dorsal portion of the LG (LGd; B) and LGv (C). **D**: FMRP staining appears stronger in the medial habenula (MH) than the lateral habenula (LH). **E,F**: Closer looks of the neurons in the LH (E) and MH (F). Note FMRP intensity at the individual cell level is comparable between these two cell groups, although MH has a higher cell density. Dashed lines outline the approximate location of different cell groups. Scale bars = 500 μm in A (applies to A,D); 50 μm in F (applies to B,C,E,F).

groups with strong FMRP expression in the brainstem, midbrain, and thalamus. Many of these cell groups are involved in fundamental sensory information processing, including auditory, visual, and somatosensory, or in motor control. It is important to note that not all sensory and motor neurons at these subcortical levels are normally rich in FMRP. Most auditory and somatosensory nuclei in the brainstem, midbrain, and thalamus strongly express FMRP. Visual nuclei, on the other hand, exhibit a more selected manner of FMRP expression. Consistent with previous observation in primates (Kogan et al., 2004a), high levels of FMRP are seen in the mouse dorsolateral geniculate nucleus, the major thalamic target of the ascending pathway from the retina. In contrast, FMRP intensity is relatively low in the superficial layers of the superior colliculus, a retinal

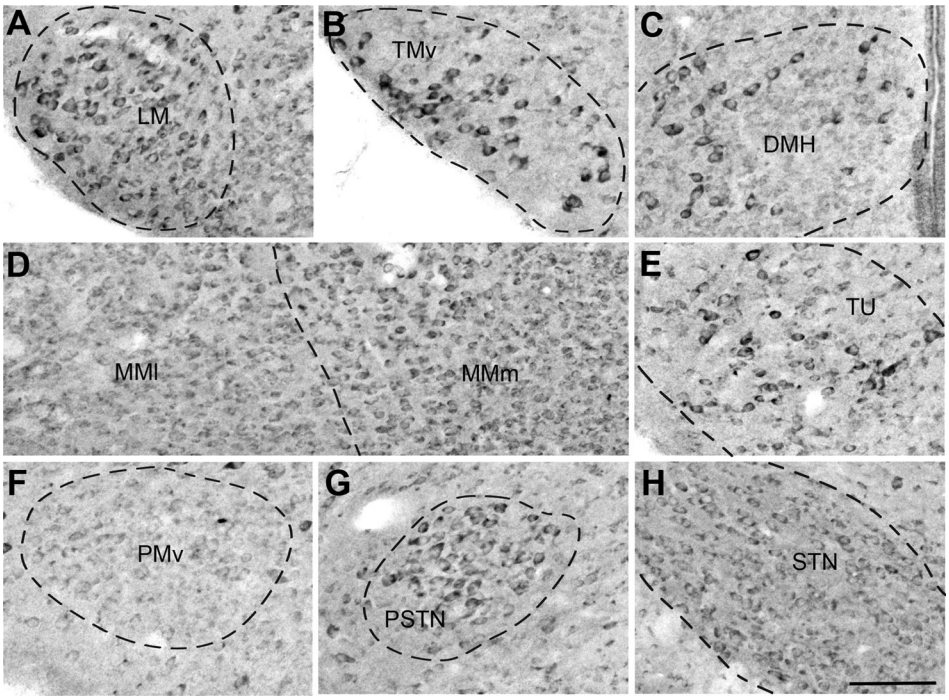

Figure 22. High-magnification images of FMRP (7G1) immunostaining in the hypothalamus. FMRP staining is strong in the lateral mammillary nucleus (LM; **A**), the ventral part of the tuberomammillary nucleus (TMv; **B**), the dorsomedial nucleus of the hypothalamus (DMH; **C**), the medial part of the medial mammillary nucleus (MMm; **D**), the tuberal nucleus (TU; **E**), the parasubthalamic nucleus (PSTN; **G**), and the subthalamic nucleus (STN; **H**). In contrast, FMRP staining is weak in the ventral premammillary nucleus (PMv; **F**). Note that FMRP staining is weaker in the lateral part of the medial mammillary nucleus (MMl) than in the MMm (D). Dashed lines outline the approximate location of different cell groups. Scale bar = 100 μm.

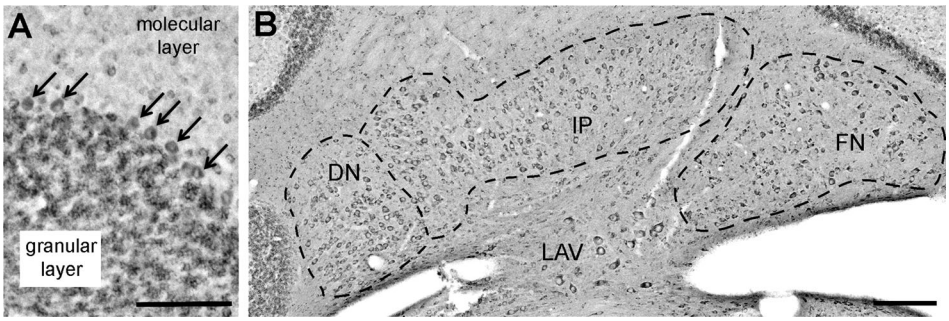

Figure 23. High-magnification images of FMRP (7G1) immunostaining in the cerebellum. **A**: Strong FMRP staining in Purkinje neurons (arrows) and granular layer but not in the molecular layer. **B**: FMRP staining in the three cerebellar nuclei. Dashed lines outline the approximate location of these nuclei. Scale bars = 100 μm in A; 200 μm in B.

target in the midbrain (Butler et al., 2011). Similarly, not all motor neurons are normally rich in FMRP. Striking differences in FMRP level are seen between the adjacent dorsal motor nucleus of the vagus nerve (DMX) and the hypoglossal nucleus (XII), two primary cell groups of cranial nerves. Taken together, FMRP is selectively expressed at high levels in subcortical sensory and motor neurons in mature brains.

If FMRP-rich sensory neurons are significant targets in FXS, one might expect to see that these neurons exhibit structural and/or functional plasticity in response to changes in neuronal activity in normal brains and that such activity-dependent plasticity is compromised when FMRP is absent. Indeed, hearing loss or abnormal hearing induced by tinnitus leads to extensive alternations in cellular properties of auditory

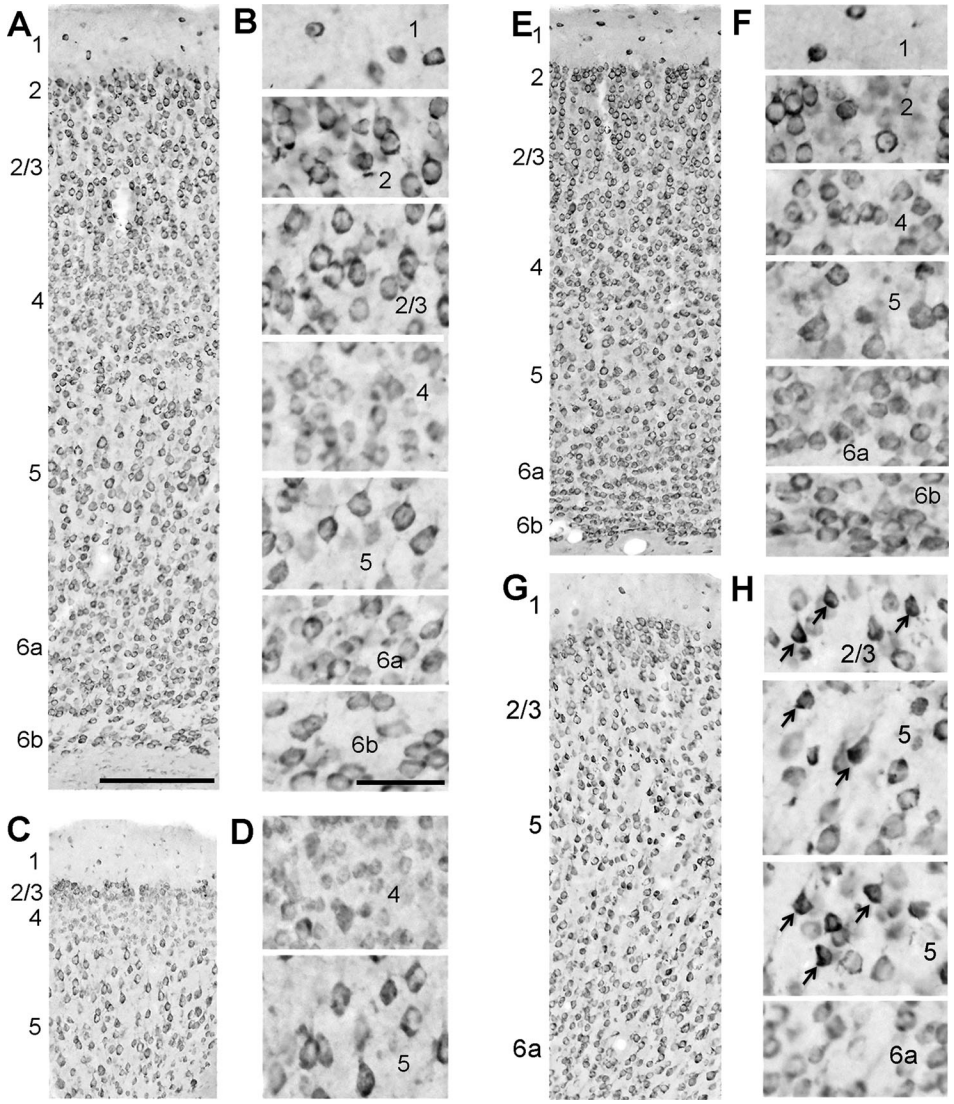

Figure 24. High-magnification images of FMRP (7G1) immunostaining in the isocortex. **A,B**: The primary somatosensory area taken from the level comparable to Fig. 12. B: Closer looks of individual layers in A. **C,D**: The ventral part of retrosplenial area taken from the level comparable to Fig. 9. D: Closer looks of individual layers in C. **E,F**: The primary visual area taken from the level comparable to Fig. 9. F: Closer looks of individual layers in E. **G,H**: The anterior cingulate area taken from the level comparable to Fig. 12. H: Closer looks of individual layers in G. Note that neurons in layer 4 are more lightly stained than other layers in the somatosensory (A,B) and retrosplenial (C,D), but not in the visual (E,F), areas. Neurons in layers 2–3 exhibit stronger staining than other layers in the somatosensory (A,B) and visual (E,F) areas. Arrowheads in H indicate the neurons with uniquely strong staining. Scale bars = 200 μm in A (applies to A,C,E,G); 50 μm in B (applies to B,D,F,H).

neurons throughout the brain (Rubel and Fritzsch, 2002; Parks and Rubel, 2004; Saunders, 2007; Berger and Coomber, 2015; Tong et al., 2015; Ryugo, 2015; Bayat et al., 2016). In FMR1 knockout mice, auditory brainstem neurons show altered synaptic connectivity and reduced activity-dependent regulation of ion channel expression and conductance (Brown and Kaczmarek, 2011; Rotschafer et al., 2015). In primates and humans, FMRP expression in the magnocellular layers of the lateral geniculate nucleus (LGN) is stronger than that in the parvocellular layers of LGN (Kogan et al., 2004a). Consistently, FXS patients show selective visual deficit of the magnocellular, but not parvocellular visual pathway, although the role of neuronal activity in this visual function is not clear. Similarly, in the olfactory bulb, where FMRP is strongly expressed, neuronal dendritic dynamics in response to alterations of sensory experience are reduced in FMR1 knockout mice (Daroles et al., 2015), including deficits in learned olfactory function (Larson et al., 2008; Sudhakaran et al., 2014; Nitenson et al., 2015).

Taken together, these studies strongly implicate the importance of FMRP regulation in selected aspects of fundamental sensory information processing in mature brains at the subcortical levels. This implication argues that there are two avenues whereby FXS can influence cortical function, where the sensory perception is thought to be generated. One is the influence of FMRP on the development and maintenance of the cortical neurons themselves. The second is through altered sensory signals they receive due to abnormal functioning and/or abnormal connectivity of sensory neurons in the brainstem, midbrain, and thalamus. Therefore, in addition to studies of cortical neurons, investigations of

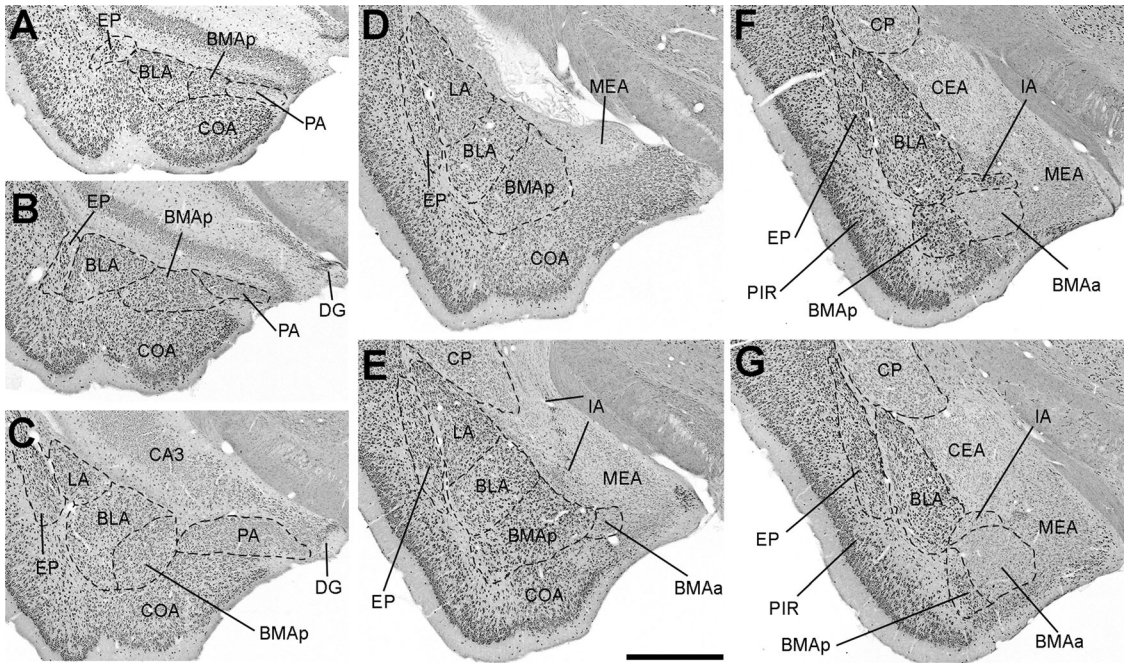

Figure 25. High-magnification images of FMRP (7G1) immunostaining in the cortical subplate and striatum. **A–G**: Serials images throughout the cortical subplate from caudal (A) to rostral (G). Dashed lines outline the approximate boundaries of a number of nuclei. Scale bar = 500 μm.

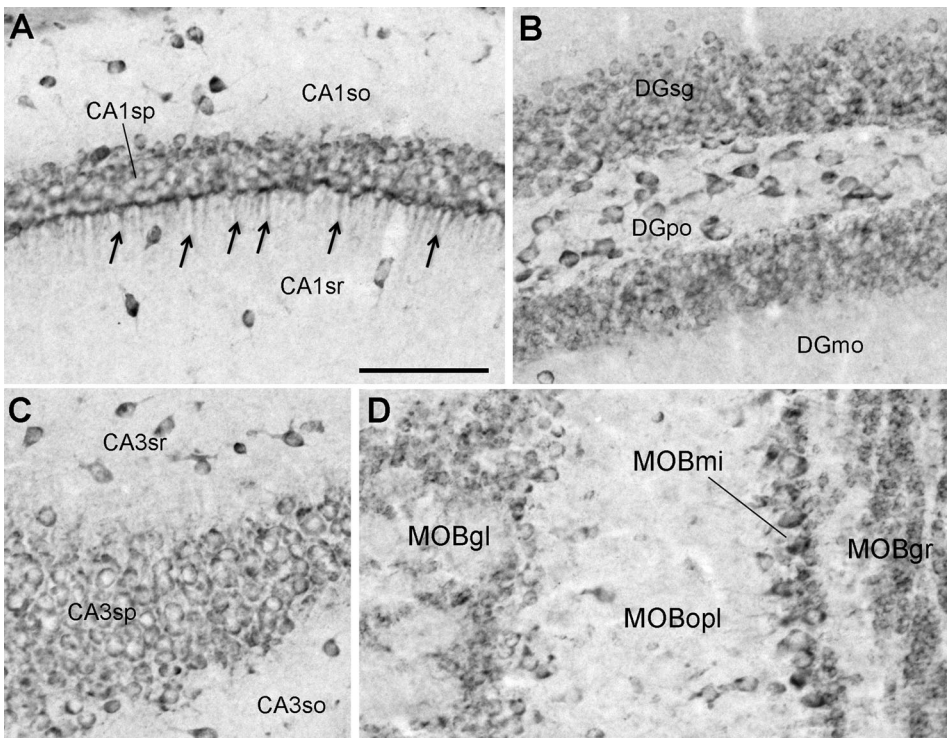

Figure 26. High-magnification images of FMRP (7G1) immunostaining in the hippocampus and the main olfactory bulb (MOB). **A**: FMRP staining in the hippocampus CA1. Arrows indicate stained dendrites of the pyramidal neurons. **B**: FMRP staining in the dentate gyrus (DG). **C**: FMRP staining in the hippocampus CA3. **D**: FMRP staining in the MOB. Scale bar = 100 μm.

FMRP function at subcortical levels may be both experimentally advantageous and clinically significant; sensory processing circuits at the subcortical levels are often more thoroughly characterized and may be more conserved across vertebrate species than cortical neural circuits.

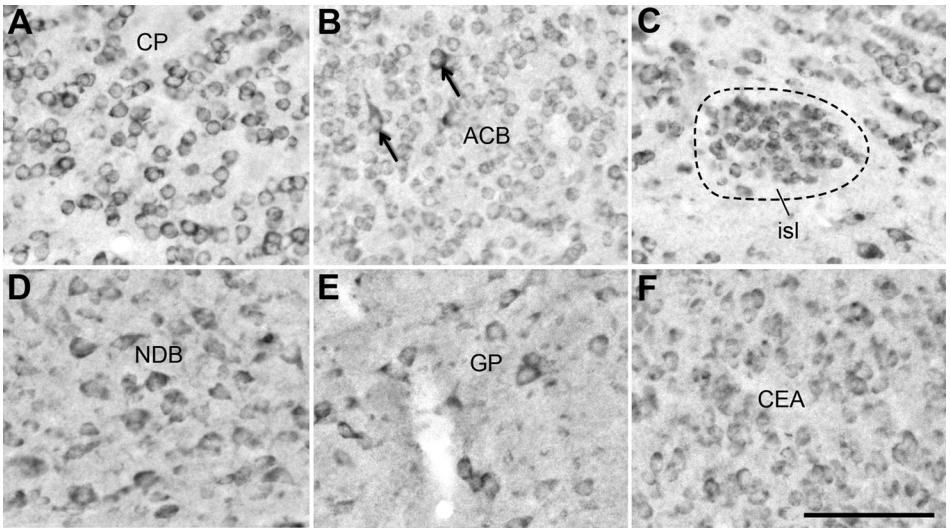

Figure 27. High-magnification images of FMRP (7G1) immunostaining in the striatum and pallidum. FMRP staining is stronger in the caudoputamen (CP; **A**), the islands of Calleja (isl; **C**), the diagonal band nucleus (NDB; **D**), and the globus pallidus (GP; **E**), than in the nucleus accumbens (ACB; **B**) and the central amygdalar nuclei (CEA; **F**). Arrows in B indicate two more darkly labeled neurons in ACB. Dashed line in C outlines the boundary of one island of Calleja. Scale bar = 100 μm.

Hypothalamus

The hypothalamus is in general low in FMRP in mature brains with the exception of a number of cell groups of the mammillary body. The mammillary body is closely related to the hippocampus and plays an important role in spatial memory (Vann and Nelson, 2015). The finding of a high FMRP level in the mammillary body is of particular interest in light of memory and learning deficits in FXS individuals and extensive documentation on reduced neuronal plasticity of hippocampal neurons in FMR1 knockout mice (Mercaldo et al., 2009). The current study found varied FMRP expression levels among distinct cell groups of the mammillary body, suggesting differential contribution of each cell group to memory deficits in FXS.

Data on neuroendocrine function of the hypothalamus are seemingly disparate. Hypothalamic nuclei are known to control food intake, body temperature, fatigue, sleep, and circadian rhythms (Bakos et al., 2016). A number of neuroendocrine studies implicated hypothalamic dysfunction in FXS, including abnormal activation of the hypothalamic–pituitary–adrenal axis (Hessl et al., 2004). In addition, significantly reduced neuronal activity was reported in the hypothalamus of FMR1 knockout mice of 5-week-old mice (Michalon et al., 2013). These studies may help to explain the abnormal stress responses, sleep abnormalities, and physical growth patterns commonly seen in affected individuals (Bregman et al., 1990; Hessl et al., 2004). Low FMRP expression in most hypothalamic nuclei at comparable ages appears inconsistent with these behavioral studies. This could also be showing us one of the differences in FMRP expression in mice and human brains. Alternatively, it may suggest the importance of FMRP to hypothalamus during development rather than at relatively more mature stages. Consistent with this idea is the significant increase in the gray matter volume in hypothalamus found in 1–3-year-old (Hoeft et al., 2008) but not older (Gothelf et al., 2008) children with FXS based on magnetic resonance imaging studies. It is clear that further research is needed to consolidate these seemingly disparate findings, but it does raise the possibility that FMRP may be differentially expressed at different levels in developing hypothalamic nuclei.

Cortex layer 4

Reduced neuronal plasticity of various cortical cell types is repeatedly reported in FMR1 knockout animals (for example, Li et al., 2002; Gocel et al., 2012; Padmashri et al., 2013; Yang et al., 2014; Koga et al., 2015; Martin et al., 2016; Nagaoka et al., 2016). FMRP is strongly expressed in almost all layers throughout the neocortex in mature brains. However, the FMRP protein level is not uniform. For example, small granule neurons of layer 4, the primary cortical targets of ascending thalamic inputs, exhibit significantly lower FMRP levels as compared to other layers in area 29 and some somatosensory areas. Interestingly, layer 4 is uniquely highly developed in area 29, with a

corresponding reduction of layers 2 and 3 (Brodmann, 1909). Area 29, a portion of the retrosplenial cortex, is thought to participate in memory, navigation, and other cognitive functions (Vann et al., 2009). In the somatosensory area, Till et al. (2012) reported alterations in dendritic and spine morphology of spiny stellate neurons of layer 4. Whether structural changes occur to small granule cells in the same layer is unknown, probably due to the difficulty of studying this cell type (see discussion in Wang et al., 2010). Layer-specific expression of FMRP is also found in another laminar structure, the superior colliculus. Although the significance and implications of these differential expression patterns in FMRP neurobiology and FXS pathology are unknown, it amplifies the importance of studying FMRP mechanisms with the resolution of individual layers and cell types.

CONCLUSION

The findings presented in this study provide fundamental background information for understanding FMRP function in the mature brain. Additional complementary studies assessing cellular distribution patterns at critical developmental stages will be essential for exploring specific contribution of various FMRP regulatory mechanisms to normal brain function. In addition, our findings emphasize the need and advantages of studying sensory information processing at subcortical levels for understanding FMRP functions in normal and FXS brains.

ACKNOWLEDGMENT

We thank Mr. Dale Cunningham for technical support.

CONFLICT OF INTEREST

The authors have no identified conflicts of interest.

ROLE OF AUTHORS

All authors had full access to all the data in the study and take responsibility for the integrity of the data and the accuracy of the data analysis. Study concept and design: Wang Y and Rubel EW. Acquisition and analysis of data: Wang Y, Jackson C, Yong L, Zorio D. Drafting of the article: Zorio D, Wang Y. Obtained funding: Wang Y.

DATA ACCESSIBILITY

Upon acceptance of the article, the complete series of high-resolution images of FMRP (7G1) immunostaining will be deposited onto the Biolucida Cloud server maintained by MBF Biosciences.

LITERATURE CITED

Abitbol M, Menini C, Delezoide AL, Rhyner T, Vekemans M, Mallet J. 1993. Nucleus basalis magnocellularis and hippocampus are the major sites of FMR-1 expression in the human fetal brain. Nat Genet 4:147–153.

Akins MR, Leblanc HF, Stackpole EE, Chyung E, Fallon JR. 2012. Systematic mapping of fragile X granules in the mouse brain reveals a potential role for presynaptic FMRP in sensorimotor functions. J Comp Neurol 520: 3687–3706.

Bagni C, Tassone F, Neri G, Hagerman R. 2012. Fragile X syndrome: causes, diagnosis, mechanisms and therapeutics. J Clin Invest 122:4314–4322.

Bakker CE, Verheij C, Willemsen R, Vanderhelm, R, Oerlemans F, Vermey M, Bygrave A, Hoogeveen AT, Oostra BA, Reyniers E, DeBoulle K, Dhooge R, Cras P, Van Velzen N, Nagels G, Martin JJ, Dedeyn PP, Darby JK, Willems PJ. 1994. Fmr1 knockout mice: a model to study fragile X mental retardation. The Dutch-Belgian Fragile X Consortium. Cell 78:23–33.

Bakker CE, de Diego Otero Y, Bontekoe C, Raghoe P, Luteijn T, Hoogeveen AT, Oostra BA, Willemsen R. 2000. Immunocytochemical and biochemical characterization of FMRP, FXR1P and FXR2P in the mouse. Exp Cell Res 258:162–170.

Bakos J, Zatkova M, Bacova Z, Ostatnikova D. 2016. The role of hypothalamic neuropeptides in neurogenesis and neuritogenesis. Neural Plast 2016:3276383.

Bayat A, Farhadi M, Emamdjomeh H, Saki N, Mirmomeni G, Rahim F. 2016. Effect of conductive hearing loss on central auditory function. Braz J Otorhinolaryngol S1808-8694(16):30046–5.

Beebe K, Wang Y, Kulesza R. 2014. Distribution of fragile X mental retardation protein in the human auditory brainstem. Neuroscience 273:79–91.

Berger JI, Coomber B. 2015. Tinnitus-related changes in the inferior colliculus. Front Neurol 6:61.

Bledsoe SC Jr, Snead CR, Helfert RH, Prasad V, Wenthold RJ, Altschuler RA. 1990. Immunocytochemical and lesion studies support the hypothesis that the projection from the medial nucleus of the trapezoid body to the lateral superior olive is glycinergic. Brain Res 517:189–194.

Brackett DM, Qing F, Amieux PS, Sellers DL, Horner PJ, Morris DR. 2013. FMR1 transcript isoforms: association with polyribosomes; regional and developmental expression in mouse brain. PLoS One 8:e58296.

Braun K, Segal M. 2000. FMRP involvement in formation of synapses among cultured hippocampal neurons. Cereb Cortex 10:1045–52.

Bregman JD, Leckman JF, Ort SI. 1990. Thyroid function in fragile-X syndrome males. Yale J Biol Med 63:293–299.

Brodmann K. 1909. Localisation in the cerebral cortex. Translated and Edited by Garey LJ, 3rd ed. New York: Springer.

Brown MR, Kaczmarek LK. 2011. Potassium channel modulation and auditory processing. Hear Res 279:32–42.

Brown MC, Ledwith JV 3rd. 1990. Projections of thin (type-II) and thick (type-I) auditory-nerve fibers into the cochlear nucleus of the mouse. Hear Res 49:105–118

Brown V, Jin P, Ceman S, Darnell JC, O'Donnell WT, Tenenbaum SA, Jin X, Feng Y, Wilkinson KD, Keene JD, Darnell RB, Warren ST. 2001. Microarray identification of FMRP-associated brain mRNAs and altered mRNA translational profiles in fragile X syndrome. Cell 107:477–487.

Butler AB, Reiner A, Karten HJ. 2011. Evolution of the amniote pallium and the origins of mammalian neocortex. Ann N Y Acad Sci 1225:14–27.

Chaudhury S, Sharma V, Kumar V, Nag TC, Wadhwa S. 2016. Activity-dependent synaptic plasticity modulates the critical phase of brain development. Brain Dev 38:355–363.

Chen L, Toth M. 2001. Fragile X mice develop sensory hyperreactivity to auditory stimuli. Neuroscience 103:1043–1050.

Christie SB, Akins MR, Schwob JE, Fallon JR. 2009. The FXG: a presynaptic fragile X granule expressed in a subset of developing brain circuits. J Neurosci 29:1514–1524.

Cook D, Nuro E, Murai KK. 2014. Increasing our understanding of human cognition through the study of Fragile X Syndrome. Dev Neurobiol 74:147–177.

Daroles L, Gribaudo S, Doulazmi M, Scotto-Lomassese S, Dubacq C, Mandairon N, Greer CA, Didier A, Trembleau A, Caillé I. 2015. Fragile X mental retardation protein and dendritic local translation of the alpha subunit of the calcium/calmodulin-dependent kinase II messenger RNA are required for the structural plasticity underlying olfactory learning. Biol Psychiatry s0006-3223(15):00642–3.

Deng PY, Rotman Z, Blundon JA, Cho Y, Cui J, Cavalli V, Zakharenko SS, Klyachko VA.. 2013. FMRP regulates neurotransmitter release and synaptic information transmission by modulating action potential duration via BK channels. Neuron 77:696–711.

Devys D, Lutz Y, Rouyer N, Bellocq JP, Mandel JL. 1993. The FMR-1 protein is cytoplasmic, most abundant in neurons and appears normal in carriers of a fragile X premutation. Nat Genet 4:335–340.

Edwards SB, Ginsburgh CL, Henkel CK, Stein BE. 1979. Sources of subcortical projections to the superior colliculus in the cat. J Comp Neurol 184:309–329.

Feng Y, Gutekunst CA, Eberhart DE, Yi H, Warren ST, Hersch SM. 1997. Fragile X mental retardation protein: nucleocytoplasmic shuttling and association with somatodendritic ribosomes. J Neurosci 17:1539–1547.

Fisch GS, Hao HK, Bakker C, Oostra BA. 1999. Learning and memory in the FMR1 knockout mouse. Am J Med Genet 84:277–282.

Gabel LA, Won S, Kawai H, McKinney M, Tartakoff AM, Fallon JR. 2004. Visual experience regulates transient expression and dendritic localization of fragile X mental retardation protein. J Neurosci 24:10579–10583.

Galvez R, Gopal AR, Greenough WT. 2003. Somatosensory cortical barrel dendritic abnormalities in a mouse model of the fragile X mental retardation syndrome. Brain Res 971:83–89.

Galvez R, Smith RL, Greenough WT. 2005. Olfactory bulb mitral cell dendritic pruning abnormalities in a mouse model of the Fragile-X mental retardation syndrome: further support for FMRP's involvement in dendritic development. Brain Res Dev Brain Res 157:214–216.

Gholizadeh S, Halder SK, Hampson DR. 2015. Expression of fragile X mental retardation protein in neurons and glia of the developing and adult mouse brain. Brain Res 1596:22–30.

Gocel J, Larson J. 2012. Synaptic NMDA receptor-mediated currents in anterior piriform cortex are reduced in the adult fragile X mouse. Neuroscience 221:170–181.

Gothelf D, Furfaro JA, Hoeft F, Eckert MA, Hall SS, O'Hara R, Erba HW, Ringel J, Hayashi KM, Patnaik S, Golianu B, Kraemer HC, Thompson PM, Piven J, Reiss AL. 2008. Neuroanatomy of fragile X syndrome is associated with aberrant behavior and the fragile X mental retardation protein (FMRP). Ann Neurol 63:40–51.

Graybiel AM. 1978. A satellite system of the superior colliculus: the parabigeminal nucleus and its projections to the superficial collicular layers. Brain Res 145:365–374.

Hessl D, Rivera SM, Reiss AL. 2004. The neuroanatomy and neuroendocrinology of fragile X syndrome. Ment Retard Dev Disabil Res Rev 10:17–24.

Hinds HL, Ashley CT, Sutcliffe JS, Nelson DL, Warren ST, Housman DE, Schalling M. 1993. Tissue specific expression of FMR-1 provides evidence for a functional role in fragile X syndrome. Nat Genet 3:36–43.

Hinton VJ, Brown WT, Wisniewski K, Rudelli RD. 1991. Analysis of neocortex in three males with the fragile X syndrome. Am J Med Genet 41:289–294.

Hoeft F, Lightbody AA, Hazlett HC, Patnaik S, Piven J, Reiss AL. 2008. Morphometric spatial patterns differentiating boys with fragile X syndrome, typically developing boys and developmentally delayed boys aged 1 to 3 years. Arch Gen Psychiatry 65:1087–1097.

Irwin SA, Patel B, Idupulapati M, Harris JB, Crisostomo RA, Larsen BP, Kooy F, Willems PJ, Cras P, Kozlowski PB, Swain RA, Weiler IJ, Greenough WT. 2001. Abnormal dendritic spine characteristics in the temporal and visual cortices of patients with fragile-X syndrome: a quantitative examination. Am J Med Genet 98:161–167.

Irwin SA, Idupulapati M, Gilbert ME, Harris JB, Chakravarti AB, Rogers EJ, Crisostomo RA, Larsen BP, Mehta A, Alcantara CJ, Patel B, Swain RA, Weiler IJ, Oostra BA, Greenough WT. 2002. Dendritic spine and dendritic field characteristics of layer V pyramidal neurons in the visual cortex of fragile-X knockout mice. Am J Med Genet 111: 140–146.

Khandjian EW, Fortin A, Thibodeau A, Tremblay S, Côté F, Devys D, Mandel JL, Rousseau F. 1995. A heterogeneous set of FMR1 proteins is widely distributed in mouse tissues and is modulated in cell culture. Hum Mol Genet 4: 783–789.

Koga K, Liu MG, Qiu S, Song Q, O'Den G, Chen T, Zhuo M. 2015. Impaired presynaptic long-term potentiation in the anterior cingulate cortex of Fmr1 knock-out mice. J Neurosci 35:2033–2043.

Kogan CS, Bertone A, Cornish K, Boutet I, Der Kaloustian VM, Andermann E, Faubert J, Chaudhuri A. 2004a. Integrative cortical dysfunction and pervasive motion perception deficit in fragile X syndrome. Neurology 63: 1634–1639.

Kogan CS, Boutet I, Cornish K, Zangenehpour S, Mullen KT, Holden JJ, Der Kaloustian VM, Andermann E, Chaudhuri A. 2004b. Differential impact of the FMR1 gene on visual processing in fragile X syndrome. Brain 127:591–601.

La Fata G, Gärtner A, Domínguez-Iturza N, Dresselaers T, Dawitz J, Poorthuis RB, Averna M, Himmelreich U, Meredith RM, Achsel T, Dotti CG, Bagni C. 2014. FMRP regulates multipolar to bipolar transition affecting neuronal migration and cortical circuitry. Nat Neurosci 17: 1693–1700.

Lai JK, Lerch JP, Doering LC, Foster JA, Ellegood J. 2016. Regional brain volumes changes in adult male FMR1-KO mouse on the FVB strain. Neuroscience 318:12–21.

Larson J, Kim D, Patel RC, Floreani C. 2008. Olfactory discrimination learning in mice lacking the fragile X mental retardation protein. Neurobiol Learn Mem 90:90–102.

Levenga J, de Vrij FM, Buijsen RA, Li T, Nieuwenhuizen IM, Pop A, Oostra BA, Willemsen R. 2011. Subregion-specific dendritic spine abnormalities in the hippocampus of Fmr1 KO mice. Neurobiol Learn Mem 95:467–472.

Li J, Pelletier MR, Perez Velazquez JL, Carlen PL. 2002. Reduced cortical synaptic plasticity and GluR1 expression associated with fragile X mental retardation protein deficiency. Mol Cell Neurosci 19:138–151.

Martin HG, Lassalle O, Brown JT, Manzoni OJ. 2016. Age-dependent long-term potentiation deficits in the

prefrontal cortex of the Fmr1 knockout mouse model of Fragile X Syndrome. Cereb Cortex 26:2084–2092.
McKinney BC, Grossman AW, Elisseou NM, Greenough WT. 2005. Dendritic spine abnormalities in the occipital cortex of C57BL/6 Fmr1 knockout mice. Am J Med Genet B Neuropsychiatr Genet 136:98–102.
Mercaldo V, Descalzi G, Zhuo M. 2009. Fragile X mental retardation protein in learning-related synaptic plasticity. Mol Cells 28:501–507.
Michalon A, Bruns A, Risterucci C, Honer M, Ballard TM, Ozmen L, Jaeschke G, Wettstein JG, von Kienlin M, Künnecke B, Lindemann L. 2013. Chronic metabotropic glutamate receptor 5 inhibition corrects local alterations of brain activity and improves cognitive performance in fragile X mice. Biol Psychiatry 75:189–197.
Nagaoka A, Takehara H, Hayashi-Takagi A, Noguchi J, Ishii K, Shirai F, Yagishita S, Akagi T, Ichiki T, Kasai H. 2016. Abnormal intrinsic dynamics of dendritic spines in a fragile X syndrome mouse model in vivo. Sci Rep 6:26651.
Nitenson AS, Stackpole EE, Truszkowski TL, Midroit M, Fallon JR, Bath KG. 2015. Fragile X mental retardation protein regulates olfactory sensitivity but not odorant discrimination. Chem Senses 40:345–350.
Padmashri R, Reiner BC, Suresh A, Spartz E, Dunaevsky A. 2013. Altered structural and functional synaptic plasticity with motor skill learning in a mouse model of fragile X syndrome. J Neurosci 33:19715–19723.
Parks TN, Rubel EW. 2004. Plasticity of the auditory system, vol 23. In: Popper AN, Fay RR, editors. Springer handbook of auditory research. New York: Springer.
Paxinos G, Franklin KBJ. 2013. The mouse brain in stereotaxic coordinates, 4th ed. Cambridge, MAAcademic Press .
Penagarikano O, Mulle JG, Warren ST. 2007. The pathophysiology of fragile X syndrome. Annu Rev Genomics Hum Genet 8:109–129.
Pietropaolo S, Guilleminot A, Martin B, D'Amato FR, Crusio WE. 2011. Genetic-background modulation of core and variable autistic-like symptoms in Fmr1 knock-out mice. PLoS One 6:e17073.
Rosen JB. 2004. The neurobiology of conditioned and unconditioned fear: a neurobehavioral system analysis of the amygdala. Behav Cogn Neurosci Rev 3:23–41.
Rotschafer SE, Marshak S, Cramer KS. 2015. Deletion of Fmr1 alters function and synaptic inputs in the auditory brainstem. PLoS One 10:e0117266.
Rubel EW, Fritzsch BF. 2002. Auditory system development: primary auditory neurons and their targets. Annu Rev Neurosci 25:51–101.
Rudelli RD, Brown WT, Wisniewski K, Jenkins EC, Laure-Kamionowska M, Connell F, Wisniewski HM. 1985. Adult fragile X syndrome. Clinico-neuropathologic findings. Acta Neuropathol 67:289–295.
Ryugo D. 2015. Auditory neuroplasticity, hearing loss and cochlear implants. Cell Tissue Res 361:251–269.
Saito K, Barber R, Wu J, Matsuda T, Roberts E, Vaughn JE. 1974. Immunohistochemical localization of glutamate decarboxylase in rat cerebellum. Proc Natl Acad Sci U S A 71:269–273.
Santoro MR, Bray SM, Warren ST. 2012. Molecular mechanisms of fragile X syndrome: a twenty-year perspective. Annu Rev Pathol 7:219–245.
Saunders JC. 2007. The role of central nervous system plasticity in tinnitus. J Commun Disord 40:313–334.
Schwaller B, Meyer M, Schiffmann S. 2002. 'New' functions for 'old' proteins: the role of the calcium-binding proteins calbindin D-28k, calretinin and parvalbumin, in cerebellar physiology. Studies with knockout mice. Cerebellum 1: 241–258.
Sinclair D, Oranje B, Razak KA, Siegel SJ, Schmid S. 2016. Sensory processing in autism spectrum disorders and Fragile X syndrome–from the clinic to animal models. Neurosci Biobehav Rev S0149-7634(15)30318–3.
Strumbos JG, Brown MR, Kronengold J, Polley DB, Kaczmarek LK. 2010. Fragile X mental retardation protein is required for rapid experience-dependent regulation of the potassium channel Kv3.1b. J Neurosci 30: 10263–10271.
Sudhakaran IP1, Hillebrand J, Dervan A, Das S, Holohan EE, Hülsmeier J, Sarov M, Parker R, VijayRaghavan K, Ramaswami M. 2014. FMRP and Ataxin-2 function together in long-term olfactory habituation and neuronal translational control. Proc Natl Acad Sci U S A 111:E99–E108.
Telias M, Segal M, Ben-Yosef D. 2013. Neural differentiation of fragile X human embryonic stem cells reveals abnormal patterns of development despite successful neurogenesis. Dev Biol 374:32–45.
Tessier CR, Broadie K. 2008. Drosophila fragile X mental retardation protein developmentally regulates activity-dependent axon pruning. Development 135:1547–1557.
Till SM. 2010. The developmental roles of FMRP. Biochem Soc Trans 38:507–510.
Till SM, Wijetunge LS, Seidel VG, Harlow E, Wright AK, Bagni C, Contractor A, Gillingwater TH, Kind PC. 2012. Altered maturation of the primary somatosensory cortex in a mouse model of fragile X syndrome. Hum Mol Genet 21: 2143–2156.
Tong L, Strong MK, Kaur T, Juiz JM, Oesterle EC, Hume C, Warchol ME, Palmiter RD, Rubel EW. 2015. Selective deletion of cochlear hair cells causes rapid age-dependent changes in spiral ganglion and cochlear nucleus neurons. J Neurosci 35:7878–7891.
Thomas CC, Combe CL, Dyar KA, Inglis FM. 2008. Modest alterations in patterns of motor neuron dendrite morphology in the Fmr1 knockout mouse model for fragile X. Int J Dev Neurosci 26:805–811.
Vann SD, Nelson AJ. 2015. The mammillary bodies and memory: more than a hippocampal relay. Prog Brain Res 219: 163–185.
Vann SD, Aggleton JP, Maguire EA. 2009. What does the retrosplenial cortex do? Nat Rev Neurosci 10:792–802.
Verheij C, de Graaff E, Bakker CE, Willemsen R, Willems PJ, Meijer N, Galjaard H, Reuser AJ, Oostra BA, Hoogeveen AT. 1995. Characterization of FMR1 proteins isolated from different tissues. Hum Mol Genet 4:895–901.
Verkerk AJMH, Pieretti M, Sutcliffe JS, Fu Y-H, Kuhl DPA, Pizzuti A, Reiner O, Richards S, Victoria MF, Zhang F, Eussen BE, van Ommen GJB, Blonden LAJ, Riggins GJ, Chastain JL, Kunst CB, Galjaard H, Caskey CT, Nelson DL, Oostra BA, Warren ST. 1991. Identification of a gene (FMR-1) containing a CGG repeat coincident with a breakpoint cluster region exhibiting length variation in fragile X syndrome. Cell 65:905–914.
Wang Y, Major DE, Karten HJ. 2004. Morphology and connections of nucleus isthmi pars magnocellularis in chicks (Gallus gallus). J Comp Neurol 469:275–297.
Wang Y, Luksch H, Brecha NC, Karten HJ. 2006. Columnar projections from the cholinergic nucleus isthmi to the optic tectum in chicks (Gallus gallus): a possible substrate for synchronizing tectal channels. J Comp Neurol 494:7–35.
Wang Y, Brzozowska-Prechtl A, Karten HJ. 2010. Laminar and columnar auditory cortex in avian brain. Proc Natl Acad Sci U S A 107:12676–12681.

Wang Y, Sakano H, Beebe K, Brown MR, de Laat R, Bothwell M, Kulesza RJ Jr, Rubel EW. 2014. Intense and specialized dendritic localization of the fragile X mental retardation protein in binaural brainstem neurons: a comparative study in the alligator, chicken, gerbil and human. J Comp Neurol 522:2107–2128.

Xu ZH, Yang Q, Ma L, Liu SB, Chen GS, Wu YM, Li XQ, Liu G, Zhao MG. 2012. Deficits in LTP induction by 5-HT2A receptor antagonist in a mouse model for fragile X syndrome. PLoS One 7:e48741.

Yang S, Yang S, Park JS, Kirkwood A, Bao S. 2014. Failed stabilization for long-term potentiation in the auditory cortex of FMR1 knockout mice. PLoS One 9:e104691.

Yu Y, Fu Y, Watson C. 2014. The inferior olive of the C57BL/6J mouse: a chemoarchitectonic study. Anat Rec (Hoboken) 297:289–300.

Zangenehpour S, Cornish KM, Chaudhuri A. 2009. Whole-brain expression analysis of FMRP in adult monkey and its relationship to cognitive deficits in fragile X syndrome. Brain Res 1264:76–84.